Forschungszentrum Karlsruhe
in der Helmholtz-Gemeinschaft

Wissenschaftliche Berichte
FZKA 7371

Irradiation Programme HFR Phase IIb – SPICE Impact testing on up to 16.3 dpa irradiated RAFM steels

Final Report for Task TW2-TTMS 001b-D05

E. Gaganidze, B. Dafferner, H. Ries, R. Rolli, H.-C. Schneider, J. Aktaa

Institut für Materialforschung
Programm Kernfusion
Association Forschungszentrum Karlsruhe / EURATOM

April 2008

Forschungszentrum Karlsruhe

in der Helmholtz-Gemeinschaft

Wissenschaftliche Berichte

FZKA 7371

Irradiation Programme HFR Phase IIb – SPICE

Impact testing on up to 16.3 dpa irradiated RAFM steels

Final Report for
Task TW2-TTMS 001b-D05

E. Gaganidze, B. Dafferner, H. Ries, R. Rolli,
H.-C. Schneider, J. Aktaa

Institut für Materialforschung
Programm Kernfusion
Association Forschungszentrum Karlsruhe / EURATOM

Forschungszentrum Karlsruhe GmbH, Karlsruhe

2008

This work, supported by the European Communities under the contract of Association between EURATOM and Forschungszentrum Karlsruhe, was carried out within the framework of the European Fusion Development Agreement. The views and opinions expressed herein do not necessarily reflect those of the European Commission.

Forschungszentrum Karlsruhe GmbH
Postfach 3640, 76021 Karlsruhe

Mitglied der Hermann von Helmholtz-Gemeinschaft
Deutscher Forschungszentren (HGF)

ISSN 0947-8620

urn:nbn:de:0005-073718

Bestrahlungsprogramm HFR Phase IIb – SPICE: Kerbschlagbiegeuntersuchungen an bis 16.3 dpa bestrahlten RAFM Stählen

Zusammenfassung

Die Untersuchung des bestrahlungsinduzierten Versprödungsverhaltens von niedrigaktivierbaren ferritisch-martensitischen (RAFM) Stählen bildet das Ziel der vorliegenden Arbeit. Die Neutronenbestrahlung bei verschiedenen Bestrahlungstemperaturen (250-450 °C) bis zu einer Schädigung von 16,3 dpa (nominell) wurde im Hoch Fluss Reaktor („High Flux Reactor“) Petten im Rahmen des HFR Phase IIb (SPICE) Bestrahlungsprogramms durchgeführt. Die Kerbschlageigenschaften wurden an miniaturisierten Charpy-V Proben (des KLST Typs) mittels der instrumentierten Kerbschlagbiegeversuche ermittelt.

Der Hauptschwerpunkt des Bestrahlungsprogramms liegt in der Untersuchung des Einflusses der Neutronenbestrahlung auf die mechanischen Eigenschaften von einem europäischen RAFM Referenzstahl für die Erste Wand des Demonstrationsreaktors (DEMO), EUROFER97, bei zwei verschiedenen Wärmebehandlungen. Die mechanischen Eigenschaften von EUROFER97 wurden mit denen von internationalen Referenzmaterialien (F82H-mod, OPTIFER-Ia, GA3X und MANET-I), welche im SPICE Projekt untersucht wurden, verglichen. Die Bestrahlungsresistenz von bis 16,3 dpa bei 250-450 °C bestrahltem EUROFER97 ist vergleichbar mit der von besten Referenz-Strukturmaterialien. Es wurde für alle untersuchten RAFM Stähle eine erhebliche Tieftemperaturversprödung ($T_{irr} \leq 300$ °C) beobachtet. Die Wärmebehandlung von EUROFER97 bei höherer Austenisierungstemperatur führt zur wesentlichen Verbesserung des Versprödungsverhaltens bei niedrigen Bestrahlungstemperaturen ($T_{irr} \leq 350$ °C). Bei $T_{irr} \geq 350$ °C liegen die Sprödbruchübergangstemperaturen (DBTT) von untersuchten niedrigaktivierbaren Stählen unterhalb von -20 °C und damit weit unterhalb der Anwendungstemperatur. Die Analyse des Verfestigungs- vs. Versprödungs- Verhaltens deutet auf die Verfestigungsdominierte Versprödung unterhalb von $T_{irr} \leq 350$ °C mit $0{,}17 \leq C_{100} \leq 0{,}53$ °C/MPa.

Oxiddispersionsgehärteter ODS EUROFER Stahl mit 0,5 wt.% Y_2O_3 wurde bei ausgewählten Temperaturen bestrahlt. Bereits im unbestrahlten Zustand zeigte ODS EUROFER keine befriedigende Kerbschlagbiegeeigenschaften, gekennzeichnet durch eine niedrige USE = 2,54 J und durch eine große DBTT = 135 °C. Die Zunahme von USE für Bestrahlungstemperaturen unterhalb von $T_{irr} \leq 350$°C deutet außerdem auf ein nicht optimiertes Herstellungsverfahren. Bei $T_{irr} = 250$ °C ist die bestrahlungsinduzierte Verschiebung der Übergangstemperatur vergleichbar mit der vom EUROFER97. Bei höheren Bestrahlungstemperaturen zeigt hingegen ODS EUROFER größere Versprödung im Vergleich zum Referenzmetall.

Die Rolle des Heliums in der Materialversprödung wurde an EUROFER97 basierten Stählen untersucht, welche mit verschiedenem Bor Gehalt (0,008-0,112 wt.%) dotiert wurden. Bor dotierte Proben zeigen zunehmende Versprödung und Abnahme der Zähigkeit mit der Zunahme des generierten Helium Gehalts. Bis zu einem Helium Gehalt von 84 appm ist bei $T_{irr} = 250$ °C Helium induzierte Versprödung auf Helium induzierte Verfestigung zurückzuführen. Höhere Helium Konzentrationen führten zu weiteren Versprödungsmechanismen zusätzlich zur Helium induzierten Verfestigung.

Abstract

The objective of this work is to study the effects of neutron irradiation on the embrittlement behavior of different reduced activation ferritic/martensitic (RAFM) steels. The irradiation was carried out in the Petten High Flux Reactor (HFR) in the framework of the HFR Phase IIb (SPICE) irradiation project at a nominal dose of 16.3 dpa and at different irradiation temperatures (250-450 °C). The impact properties are investigated by instrumented Charpy-V tests with subsize specimens (KLST-type).

The emphasis is put on the investigation of irradiation induced embrittlement and hardening of the European RAFM reference steel for the first wall of a DEMO fusion reactor, EUROFER97 under different heat treatment conditions. The mechanical properties of EUROFER97 are compared with the results on international reference steels (F82H-mod, OPTIFER-Ia, GA3X and MANET-I) included in the SPICE project. EUROFER97 irradiated up to 16.3 dpa between 250 and 450 °C showed irradiation resistance that is comparable to those of best RAFM steels. Large low temperature ($T_{irr} \leq 300$°C) embrittlement is seen for all investigated RAFM steels. Heat treatment of EUROFER97 at higher austenitizing temperature led to the reduction of embrittlement at low temperatures ($T_{irr} \leq 350$ °C). At $T_{irr} \geq 350$°C the DBTTs of the steels remain below -20°C and, hence, are well below the application temperature. Analysis of hardening vs. embrittlement behaviour indicated hardening dominated embrittlement at $T_{irr} \leq 350$°C with $0.17 \leq C_{100} \leq 0.53$ °C/MPa.

Oxygen dispersion hardened ODS EUROFER with 0.5 wt.% Y_2O_3 has been irradiated at selected irradiation temperatures. ODS EUROFER showed not satisfying impact properties already in the unirradiated condition characterized by low USE =2.54 J and large DBTT = 135°C. Furthermore, the increase of USE for irradiation temperatures below $T_{irr} \leq 350$°C indicates not optimized fabrication process. At T_{irr} =250°C neutron irradiation induced shift in DBTT is comparable to that of the base EUROFER97 steel. At higher irradiation temperatures, however, hipped ODS EUROFER shows larger embrittlement compared to base metal.

He embrittlement is investigated in EUROFER97 based steels, that are doped with different contents of natural boron and the separated ^{10}B-isotope (0.008-0.112 wt.%). Boron doped steels show progressive embrittlement and reduction of toughness with increasing helium amount. At T_{irr} =250 °C helium induced embrittlement is of hardening nature for low helium contents up to 84 appm. Larger helium concentrations lead to non-hardening embrittlement mechanisms beyond that of hardening embrittlement.

CONTENTS

LIST OF TABLES

LIST OF FIGURES

1 Introduction

Withstanding high neutron and heat flux is a crucial prerequisite for material qualification for future fusion reactors. Reduced activation ferritic/martensitic (RAFM) steels are promising structure materials for the first wall and blanket applications in future power plants. Impact properties of modified commercial 10-11%-Cr-NiMoVNb (MANET) steels as well as newly developed RAFM 7-10%-Cr-WVTa (OPTIFER, F82H) steels have been thoroughly studied within the former irradiation programs (FRUST/SIENA [1], MANITU [2],[3],[4],[5], HFR-Ia [6], HFR-Ib [6],[7]) up to an irradiation damage dose of 2.4 displacements per atom (dpa) (MANET: 15dpa) at different irradiation temperatures (250, 300, 350, 400, and 450°C). Although, newly developed RAFM steels exhibit clearly better irradiation performance compared to the modified commercial alloys, the hardening induced by neutron irradiation accompanied by embrittlement, reduction in toughness and ductility remain as a main obstacle for their application indicating the further need of material improvement.

The operating temperatures of conventional RAFM steels are limited to about 550°C. The structure materials with higher operating temperatures, however, are required in order to increase the efficiency of the future power plants. Oxide dispersion strengthened (ODS) RAFM steels are attractive candidates for structure materials with elevated operating temperatures up to approximately 650°C. Although the tensile and impact properties of selected unirradiated ODS RAFM steels seem quite satisfactory [8], their irradiation resistance requires extensive investigation.

Transmutation helium generated in the future fusion reactor structure materials exposed to 14MeV neutrons is believed to strongly influence material embrittlement behaviour. The influence of helium generation on the impact toughness has been intensively investigated in MANITUE [2],[3],[4],[5] and HFR Ia, HFRIb [7] programmes by irradiation induced boron-to-helium transformation. The boron content was found to be a controlling factor for the irradiation induced embrittlement at low and medium irradiation dose levels [9],[6]. Different doping factors of alloying constituents promise to give new insights into irradiation effects on alloying elements and their relevance to the mechanical properties.

2 Irradiation Programme HFR Phase IIb – SPICE

2.1 Overview

HFR Phase IIb - SPICE (**S**am**p**le Holder for **I**rradiation of Miniaturized Steel Spe**c**im**e**ns Simultaneously at Different Temperatures) irradiation programme [10] have been carried out within the framework of the European Long-term Fusion Materials Development Programme. The aim is the development of structure materials for future fusion reactors. The SPICE irradiation programme represents a continuation of the irradiation programmes FRUST/SIENA, MANITU, HFR-Ia and HFR-Ib. In the current irradiation programme the emphasis is put on the neutron irradiation induced embrittlement and hardening of European reference steel for the first wall of a DEMO fusion reactor, 9% CrWVTa EUROFER97 which is a result of the development from OPTIFER-I to OPTIFER VII. The steel was irradiated up to a target dose

of 15 dpa at different target temperatures of 250, 300, 350, 400, and 450°C. This is the first irradiation experiment, in the course of which a damage of 15 dpa was reached at five different temperature levels simultaneously. The higher irradiation dose of 15 dpa compared to previous irradiation programmes is a step towards fusion-relevant doses. The irradiation performance of EUROFER97 is compared with the results on international reference steels also included in the irradiation programme.

To investigate irradiation resistance of ODS RAFM steels a technological variant of EUROFER97 with Y_2O_3 content of 0.5% prepared by hot isostatic pressing (HIP) process has been irradiated at selected irradiation temperatures.

A role of He in a process of non-hardening embrittlement is investigated in EUROFER97 based steels, that are doped with different contents of natural boron and the separated ^{10}B-isotope.

2.2 Steels

2.2.1 EUROFER97

An industrial batch of the European RAFM steel EUROFER97 was produced by Böhler Austria GmbH. The chemical composition of the steels along with the heat numbers are indicated in Table 8-1. Part of the specimens (labelled EUROFER97 ANL) has been machined from the 25 mm thick EUROFER97 plates in the as-delivered state (i.e. austenitizing at 980°C followed by tempering at 760°C). In order to study the influence of higher austenitizing temperature on a laboratory scale, another part of specimens (labelled EUROFER97 WB) has been machined from EUROFER97 plates subjected to a heat treatment at higher austenitizing temperature (i.e. at 1040°C). Table 8-2 lists the heat treatment conditions along with selected properties of the investigated materials.

2.2.2 Reference RAFM Steels

For comparative purpose the heat treatment conditions for the reference RAFM alloys F82H-mod, GA3X, OPTIFER-Ia and martensitic steel MANET-I were identical to those from previous irradiation experiments [5],[7]. While OPTIFER alloys can be handled as medium level waste after more than 100 years, F82H-mod and EUROFER97 can be considered as low-level radioactive.

2.2.3 ODS EUROFER

The European RAFM steel EUROFER97 was chosen for the production of two variants of ODS steels with different Y_2O_3 contents (0.3 and 0.5 wt%) [8]. The production process included inert gas atomisation of EUROFER and subsequent mechanical alloying in industrial ball mills. Hot isostatic pressing was chosen as the appropriate consolidation process for the production of four bars of each heat, 60 mm in diameter and 300 mm in length. ODS EUROFER steel with 0.5 wt% Y_2O_3 content has been included in the current irradiation programme.

2.2.4 Boron Doped Steels

Experimental heats ADS2 (OPTIFER-VIII), ADS3 and ADS4 with the basic composition of EUROFER97 are doped with different contents of natural boron and the separated ^{10}B-isotope (0.008-0.112 wt.%) to study the effects of helium generation [11]. In order to exclude significant differences in the microstructure, ADS2 and ADS3 were doped nearly with the same amount (82 wppm) of natural boron and separated ^{10}B isotope, respectively.

2.3 Charpy-V Specimen Geometry

Embrittlement behaviour and hardening of the steels have been quantified by impact testing. In order to enable a direct comparison with previously obtained results, the sub-sized Charpy-V specimens of KLST type (DIN 50115), see Fig. 2-1, have been produced parallel to the rolling direction of the material plates (L-T orientation).

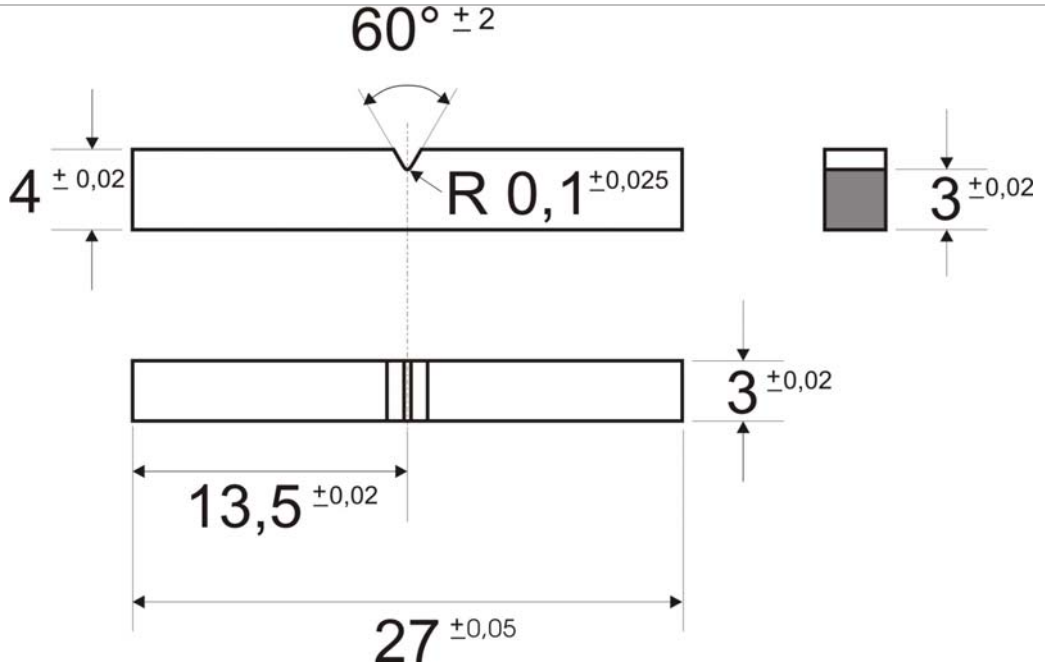

Fig. 2-1 Charpy specimen (all dimensions in mm)

2.4 Specimen Preparation and Delivery

The specimens have been fabricated by FZK's central workshop and by an external manufacturer [10]. All specimens have been measured and comply with tolerance dimensions indicated in the drawings. They are treated by ultrasonic cleaning, twice with acetone, once with alcohol.

Charpy specimens are labelled on both sides, tensile and fatigue specimens are labelled on the top side with no central hole. Charpy and tensile specimens are labelled by engraving, fatigue specimens by laser beam.

The specimens were assorted in cases, classified by materials, with clear legends, one for each sample holder and each temperature, i.e. 15 cases in total for avoiding confusion.

The specimens were handed to Dr. Casalta (European Commission – Joint Research Centre) in Petten. An associated technical documentation was delivered as well.

2.5 Irradiation Technical Details

The irradiations have been carried out by the Institute for Energy (IE) of the Joint Research Centre (JRC), Petten site, of the European Commission (EC). The SPICE project includes three simultaneous irradiation campaigns performed in the TRIO irradiation capsule, see Fig. 2-2, placed in one of the 9 in-core irradiation position C3 of the High Flux Reactor surrounded by fuel assembles [12]. The TRIO irradiation capsule was equipped with the specially designed three sodium-filled specimen holders coded as 329-01 (SPICE-C) loaded with 130 Charpy specimens, 330-01 (SPICE-T) loaded with 91 tensile specimens and 331-01 (SPICE-F) loaded with 160 fatigue specimens.

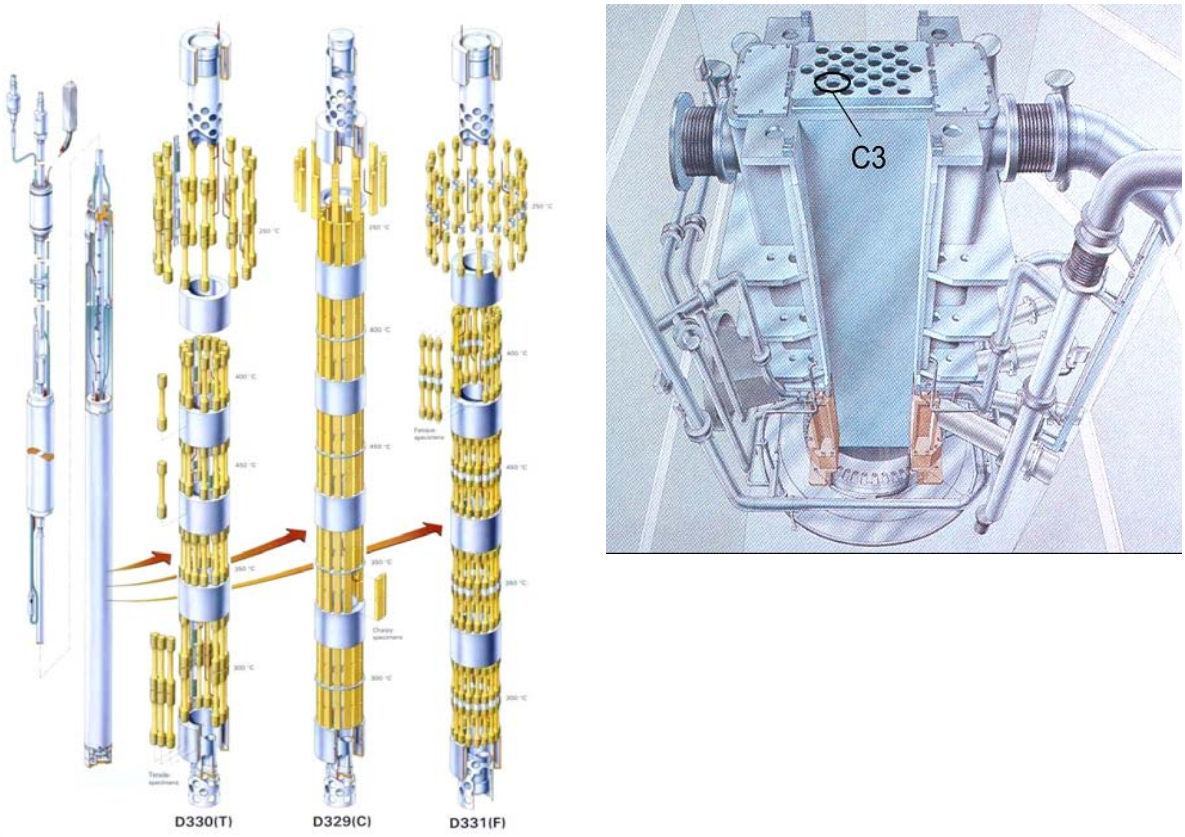

Fig. 2-2 Left: Trio irradiation capsule with three sample holders, vertical displacement unit for neutron flux control unit. Right: Reactor vessel of the High Flux Reactor, Petten. The position of the SPICE capsule which is surrounded by fuel assembles is marked.

All the three sample holders were irradiated at five different target temperatures (i.e. 250, 300, 350, 400 and 450°C) up to a target dose level of 15 dpa. Irradiation started in cycle 01-07, i.e. on 10.08.01 and ended in cycle 04-04, i.e. on 24.05.04 after 771 full power days (31 reactor operating cycles).

Each specimen holder consisted of a stainless steel construction housing the specimens under liquid sodium environment in five compartments (drums). The specimen compartments were separated by vacuum chambers (temperature barriers) in axial direction [13]. The temperature was controlled by means of gradual gas gap between the stainless steel holder and the TRIO thimble. The gas cooling medium used was a mixture of helium and neon. The operating temperature of the specimens was controlled by a vertical displacement unit (VDU) for moving the specimen holder vertically following the fluence rate shift due to control rod adjustment and by adjusting the individual gas mixtures (helium concentration), regulating heat transfer between the specimen holder and the coolant. The sample holder was equipped with 24 type-K thermocouples. 20 of them were situated in sodium environment close to the specimens at various vertical positions and remaining 4 thermocouples were situated in the upper part of the specimen holder for monitoring the sodium level. During reactor operation the centre-line of the specimen holder was situated on average 46 mm below the centre-line of the reactor core.

The liquid sodium environment provided highly improved temperature stability in comparison to the gas environment used in former HFR experiments. For the SPICE 329-01 irradiation campaign the temperature stability was satisfied for all drums except for drum 400 and 450°C. For the latter case the average deviation from the target temperature was greater than 20°C. The average irradiation temperature range for the different drums is summarised in Table 2-1.

target temperature	250°C	300°C	350°C	400°C	450°C
average temperature	244–260°C	285–301°C	339–354°C	382–400°C	386–431°C

Table 2-1: Irradiation temperatures for the five drums. The average temperature values of the four thermocouples foreseen for the monitoring of the temperature in 450°C drum were 431, 394, 386 and 410°C [12]. “Average” is the sum of all temperature values divided by the total number of readings.

One of the specimen holders (SPICE-T), irradiated in TRIO-channel 02, was instrumented with six neutron activation monitor sets delivered by NRG, Petten [14]. Volume-averaged ‘thermal’ and fast fluence rates varied in the ranges of 0.991–1.083 and 1.947–2.091 10^{18} m^{-2} s^{-1}, respectively. Fig. 2-3 shows vertical ‘thermal’ and fast (E>1.0 MeV) neutron fluence distributions in specimen holder 330-01 (SPICE-T). The results of material damage data in specimen holder 330-01 (SPICE-T) is given in Table 2-2. The volume-averaged cumulative dpa value reached after 771 full power days was 16.29 dpa for stainless steel.

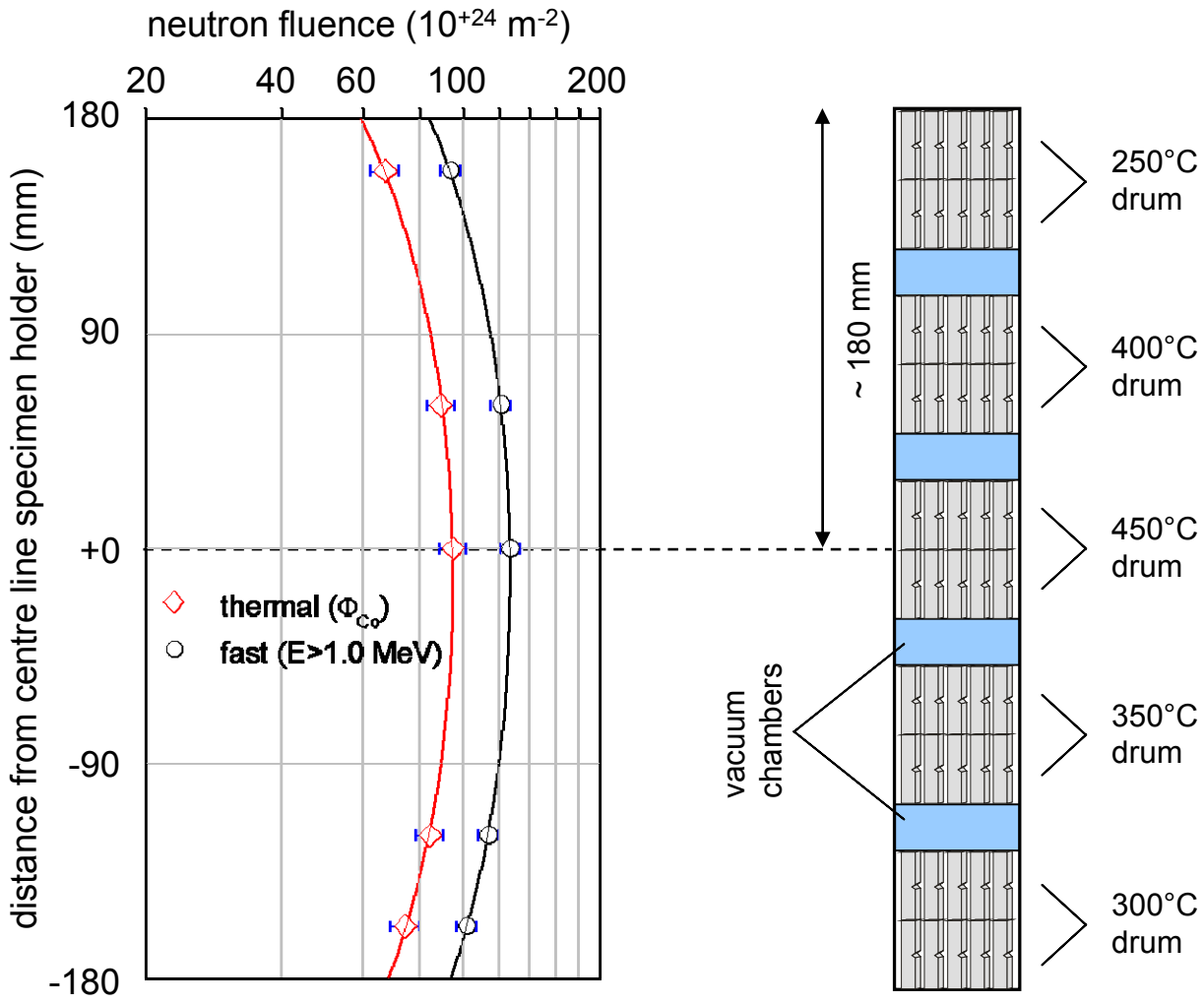

Fig. 2-3 Left: Vertical 'thermal' and fast neutron fluence distributions for specimen holder 330-01 (SPICE-T) [14]. The lines are eye-guides only. Right: Schematic representation of the loading schema of the 329-01 (SPICE-C) specimen holder.

distance to centre line specimen holder [mm]	-158	-120	+0	+60	+158
damage dose [dpa]	14.6	16.2	18.1	17.2	13.4

Table 2-2: Results of material damage data in specimen holder 330-01 (SPICE-T) [13]. Specimen material alloy – EUROFER97

Though, no neutron metrology has been done for 329-01 (SPICE-C) specimen holder, it is helpful to use the results from Table 2-2 and estimate material damage data for SPICE-C specimen holder. Performing polynomial fitting of the data from Table 2-2 and taking into account vertical position for individual drums with respect to the specimen holder centre line we estimated average dpa values received by individual drums as summarised in Table 2-3.

drum target temperature	250°C	300°C	350°C	400°C	450°C
average damage dose	13.60 dpa	14.78 dpa	17.41 dpa	16.69 dpa	18.06 dpa

Table 2-3: Estimated average material damage data for 329-01 (SPICE-C) specimen holder.

2.6 Test and Evaluation Procedure

The specimens have been transported into the hot cells of the fusion material laboratory (FML) of the institute in December 2004. The second decontamination of the specimens has been performed in the first half of 2005. The instrumented impact tests on irradiated KLST specimens have been carried out with a newly built facility installed in the hot cells. The facility is identical in construction with the one used for testing on unirradiated specimens. The test and evaluation procedures are identical with those employed in previous investigation programme [2]-[5], as summarised in Fig. 2-4.

25 J pendulum impact hammer
striker radius 2 mm
distance between supports 22 mm
impact velocity 3.85 m/s
strain gauges applied in striker
PC controlled test execution and recording
sampling rate 1 MHz
automatic specimen cooling, heating and transporting system
test temperature range between -180°C and 600°C

Fig. 2-4 Technical data for impact testing

The force vs. time curve was recorded for each experiment. For better analysis, these curves were subjected to the Fast Fourier Transformation (FFT) in order to filter out the oscillatory part in the system response. The deflection was calculated from the filtered force vs. time curves by solving the pendulum equation of motion taking into account its impact velocity. The impact energy (E) was then determined by integration of the force vs. deflection curves. The impact energies have been plotted versus test temperature (T), see e.g. Fig. 8-1, and analysed with respect to the characteristic values of the Charpy upper shelf energy (USE, i.e. maximum in the energy versus temperature diagram) and the ductile-to-brittle transition temperature (DBTT). The latter was obtained by fitting the ductile-to-brittle transition region by a hyperbolic tangent function:

$$E = \frac{LSE + USE}{2} + \frac{USE - LSE}{2} \tanh\left(\frac{T - DBTT}{r}\right) \qquad \textbf{Eq. (2-1)}$$

with LSE being the impact energy in the lower shelf, and *r* the fitting parameter related to the slope of the curve in the ductile-to-brittle transition region. In those few cases where the shape of the Charpy energy vs. test temperature curves in the ductile-to-brittle transition region deviated strongly from the hyperbolic tangent shape, the DBTT was determined as temperature at USE/2.

About 5 and 6 specimens for each material and each irradiation temperature ensured a sufficient number of measurement points for drawing the Charpy energy vs. test temperature curves.

Instrumented impact testing allowed determination of another characteristic temperature the Lowest Temperature in the Upper Shelf (LTUS), i.e. the lowest testing temperature at which material exhibits ductile behaviour. Clearly, LTUS gives the material lowest operating temperature under dynamical loading conditions comparable to those of by impact testing.

Another useful parameter obtained from the instrumented impact testing is the dynamic yield force – F_{gy}, obtained from the filtered force vs. deflection curves at the onset of plastic deformation as described in [9]. The dynamic yield stress (σ_{Dy}) was then derived according to the analytical relation [15]

$$\sigma_{Dy} = C_g \frac{M_{bgy}}{B(W - a_0)^2}$$

C_g – constraint factor (2.99)
M_{bgy} – bending moment at the onset of yield
W – specimen height (4 mm)
B – specimen thickness (3 mm)
a_0 – notch depth (1 mm).

The bending moment relates to the yield force according to

$$M_{bgy} = \frac{F_{gy}\ell}{4}$$

F_{gy} – dynamic yield force
M_{bgy} – bending moment at the onset of yield
ℓ – distance between supports (22 mm).

Impact testing of the irradiated materials started in July 2005 and finished by the end of December 2005.

3 Impact Properties

This section presents the impact properties of the investigated materials. The results of impact testing in a table form including the specimen nomenclatures and test temperatures are given in the appendix of the present report. For the sake of clarity the results on the investigated steels are presented in separate subsections for base, ODS and doped materials.

3.1 RAFM Steels

Fig. 3-1 shows the USE as a function of irradiation temperature (T_{irr}) [16],[17]. All RAFM steels show comparable USE of the order of 10 J in the unirradiated condition in clear contrast of martensitic steel MANET-I showing USE of 6.6 J. At low irradiation temperatures ($T_{irr} \leq 300°C$), the USE of EUROFER97 ANL is strongly affected by neutron irradiation, this effect being most pronounced at 300°C. The USE recovers at higher irradiation temperatures ($T_{irr} \geq 350°C$) though it still remains below the USE in the unirradiated conditions of 9.8 J. The impact toughness properties of EUROFER97 WB are influenced by 250, 350 and 450°C neutron irradiation in a quite similar way. The reference steel OPTIFER-Ia irradiated at 300°C shows the highest USE of 8.1 J, while the USE of F82H-mod irradiated at the same temperature is comparable to that of EUROFER97 ANL. MANET-I showed the worst impact toughness after neutron irradiation at 300°C. Remarkably, the impact properties on MANET-I validated the previous results obtained in the framework of the FRUST/SIENA irradiation experiment performed in 1987-1990 [1]. The results of OPTIFER-Ia, F82H-mod and GA3X irradiated at 400°C show USE comparable to that of EUROFER97 ANL.

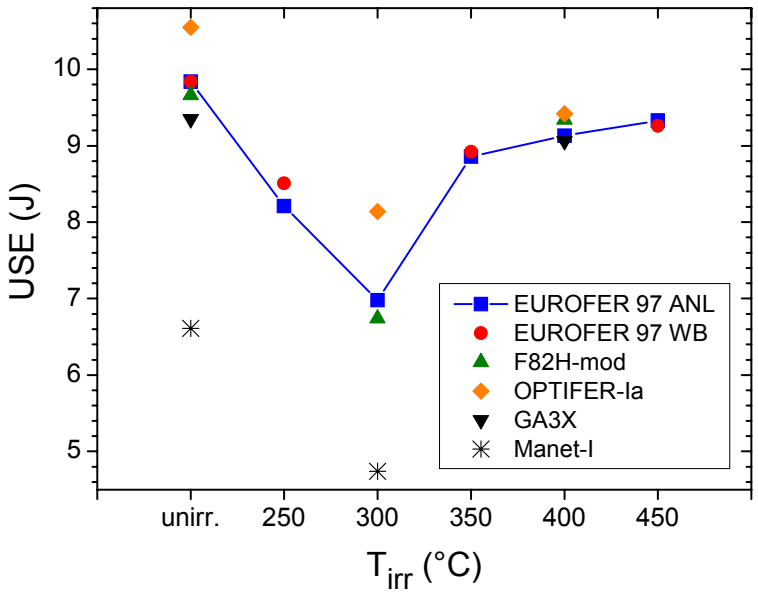

Fig. 3-1 Upper shelf energy vs. irradiation temperature (materials are indicated in figure legend). For comparison, the results in the unirradiated condition are also included.

Fig. 3-2 shows the DBTT as a function of irradiation temperature [17]. The DBTT of all materials investigated is influenced most at low irradiation temperatures ($T_{irr} \leq 300°C$). Remarkably, the DBTT of EUROFER97 WB at T_{irr} =250°C is smaller than the DBTT of EUROFER97 ANL by 50°C. The difference of the DBTTs of EUROFER97 materials austenitized at different temperatures decreases with increasing irradiation temperature and vanishes completely at 450°C. The DBTT of reference F82H-mod and OPTIFER-Ia materials is comparable to that of EUROFER97 ANL at T_{irr} =300°C. However, it has to be mentioned, that, F82H-mod

showed large impact energy scattering and correspondingly broad ductile-to-brittle-transition region in contrast to EUROFER97 ANL and OPTIFER-Ia steels, see Fig. 8-1, Fig. 8-5 and Fig. 8-7. The DBTTs of the materials irradiated above 400°C remain below -30°C and, hence, are well below the material application temperature.

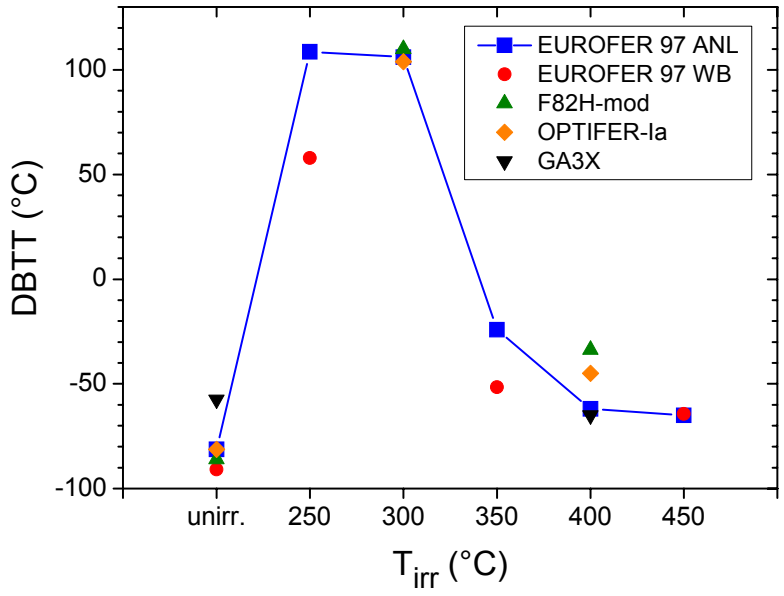

Fig. 3-2 Ductile-to-brittle transition temperature vs. irradiation temperature (materials are indicated in figure legend). For comparison, the results in the unirradiated condition are also included.

The design relevant parameter the lowest temperature in the upper shelf is presented in Fig. 3-3. In the unirradiated condition all investigated steels show comparable LTUS values with exception of GA3X which shows significantly higher LTUS value. The influence of the neutron irradiation on the LTUS is essentially similar to that on the DBTT. Moreover, nearly one to one correlation is observed between the irradiation induced shifts in the LTUS and DBTT. LTUS is mostly influenced at low irradiation temperatures ($T_{irr} \leq 300°C$). EUROFER97 WB shows better LTUS values compared to EUROFER97 ANL below $T_{irr} \leq 350°C$. The LTUSs of the both EUROFE97 steels irradiated above ($T_{irr} \geq 350°C$) remain below - 10°C. Respecting LTUS, at $T_{irr} = 400°C$ EUROFER97 ANL shows superior irradiation performance among all investigated steels. An uncertainty for OPTIFER-Ia at $T_{irr} = 400°C$ is marked by the error bar.

The hardening behaviour of the irradiated materials is shown in Fig. 3-4, where the dynamic yield stress is plotted as a function of the irradiation temperature [17]. The unirradiated values of the σ_{Dy} are also included for comparison; see also Table 8-2. Two test temperature bins have been defined for the yield stress analysis: a) RT and b) 100-120°C (nominal 100°C). At low irradiation temperatures EUROFER97 ANL shows strong hardening ($\Delta\sigma_{Dy}$) at low irradiation temperatures that is most pronounced for irradiation at 16.3 dpa/300°C. The hardening of EUROFER97 ANL is substantially reduced at higher irradiation temperatures

(T_{irr}≥ 350°C), which is in clear agreement with our previous observation at lower irradiation doses up to 2.4 dpa [5],[7].

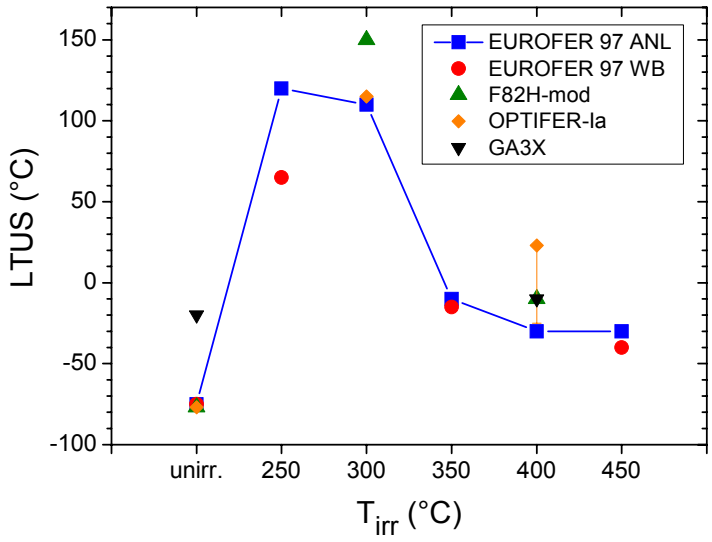

Fig. 3-3 Lowest temperature in the upper shelf vs. irradiation temperature (materials are indicated in figure legend). For comparison, the results in the unirradiated condition are also included.

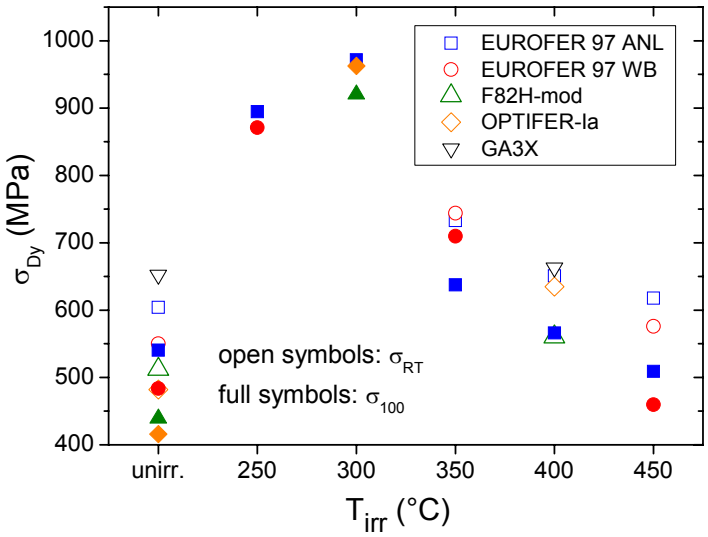

Fig. 3-4 Dynamic yield stress vs. irradiation temperature (materials are indicated in figure legend); open symbols: σ_{RT}, full symbols σ_{100}, see text for explanation. For comparison, the results in the unirradiated condition are also included.

3.2 ODS EUROFER

Fig. 3-5 shows the USE as a function of irradiation temperature (T_{irr}) for hipped ODS EUROFER. Already in the unirradiated condition ODS EUROFER shows very moderate impact toughness of 2.54 J. Furthermore, in contrast to the behaviour observed for the reference steels in Fig. 3-1, where the USE decreases at low irradiation temperatures (T_{irr} ≤300°C), the USE for ODS EUROFER is increased at T_{irr} ≤350°C compared to the unirradiated condition. At T_{irr} =450°C the USE is lower than the corresponding value in the unirradiated condition.

Fig. 3-6 shows the DBTT as a function of irradiation temperature (T_{irr}) for hipped ODS EUROFER. In the unirradiated condition DBTT lies above 100°C that is unacceptable for application as the fusion reactor structure material. DBTT is mostly influenced at T_{irr} =250°C where a shift of ~200°C observed compared to the unirradiated condition. The shift in DBTT at T_{irr} =250°C compares to the corresponding value for base EUROFER97 ANL steel of ~190°C. Above T_{irr} ≥350°C the DBTT is decreasing in qualitative agreement with the reference steels.

Fig. 3-7 shows the LTUS as a function of irradiation temperature (T_{irr}) for hipped ODS EUROFER. LTUS shows essentially the same behaviour as DBTT being mostly influenced by neutron irradiation at T_{irr} =250°C.

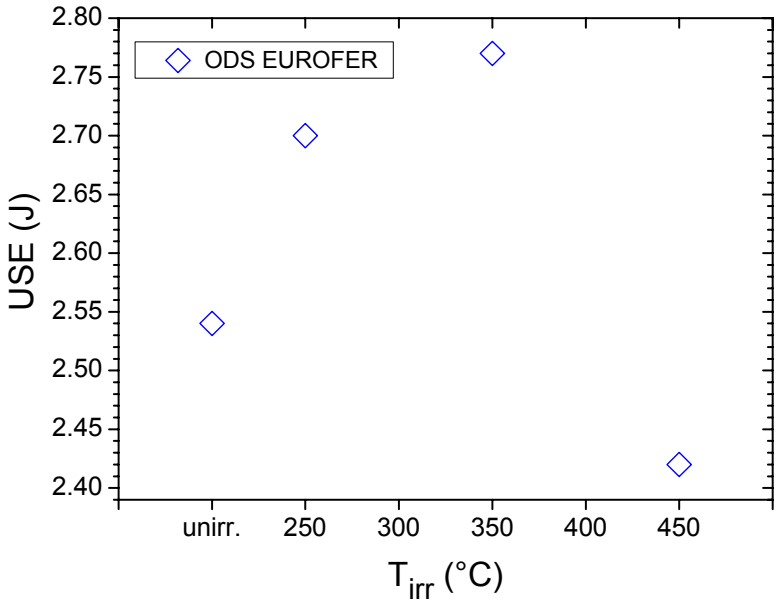

Fig. 3-5 Upper shelf energy vs. irradiation temperature for hipped ODS EUROFER. The result in the unirradiated condition is also included.

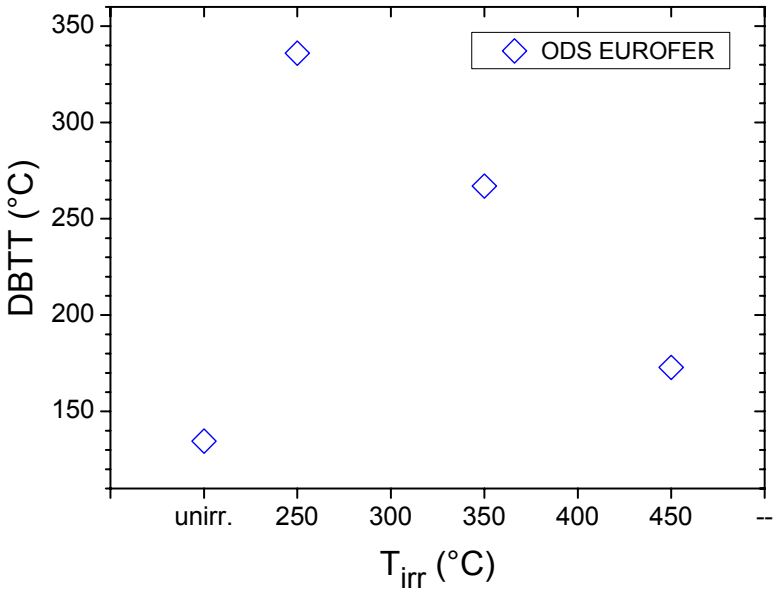

Fig. 3-6 Ductile-to-brittle transition temperature vs. irradiation temperature for hipped ODS EUROFER. The result in the unirradiated condition is also included.

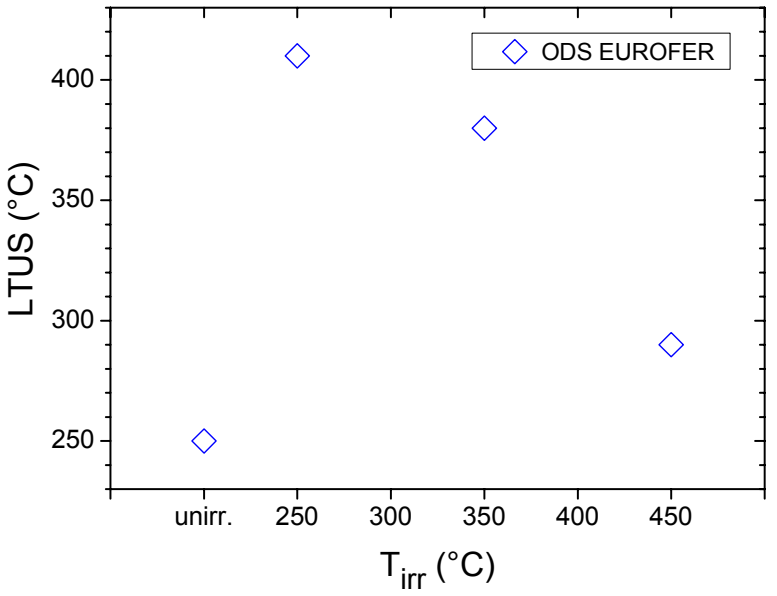

Fig. 3-7 Lowest temperature in the upper shelf vs. irradiation temperature for hipped ODS EUROFER. The result in the unirradiated condition is also included.

Fig. 3-8 shows the dynamic yield stress as a function of irradiation temperature for hipped ODS EUROFER. Since the instrumented impact testing is not well suited for the determination of the dynamic yield stress in the brittle material state the dynamic yield stress is compared at 350°C (σ_{350}) for the unirradiated and irradiated conditions.

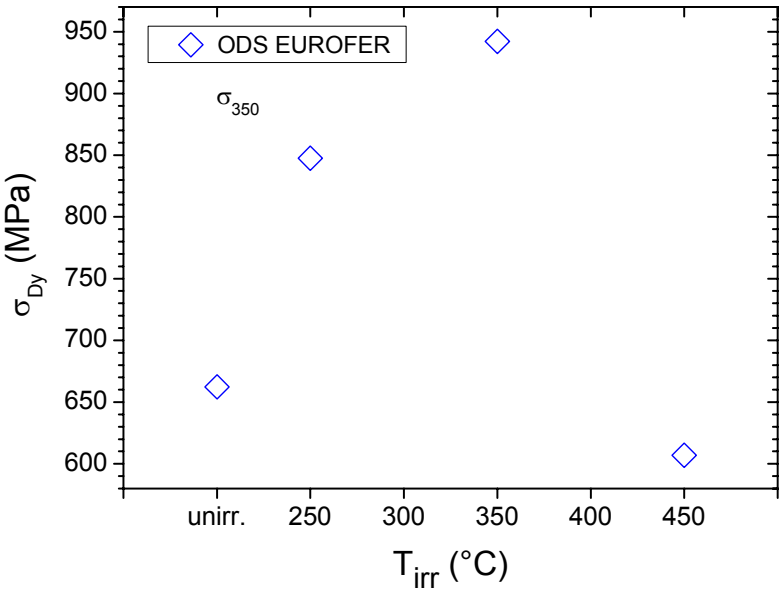

Fig. 3-8 Dynamic yield stress vs. irradiation temperature for hipped ODS EUROFER at test temperature of 350°C. The result in the unirradiated condition is also included.

3.3 Boron Doped Steels

Fig. 3-9 shows the USE as a function of irradiation temperature for doped EUROFER97 steels for two dopant constitutions of 82 wppm natural boron (ADS2) and 83 wppm separated ^{10}B isotope (ADS3). In the unirradiated condition both steels show comparable USE of the order of 9 J, that is only slightly (by ~0.9 J) lower than the USE of base EUROFER97 steel. This indicates only small chemical effects of Boron on the toughness properties. Irradiation at T_{irr} =250°C leads to a strong decrease in the USE for both steels that is more pronounced for ADS3. At T_{irr} =350°C the USE of ADS2 is nearly recovered, whereas the USE of ADS3 still shows large toughness degradation. Finally, at T_{irr} =450°C the USE of ADS2 is higher than the corresponding value for the unirradiated state. The USE of ADS3, however, is still well below than the USE in the unirradiated state. EUROFER97 doped with 1120 wppm ^{10}B (ADS4) showed USE of 5.5 J in the unirradiated condition. In the irradiated conditions, however, ADS4 showed completely brittle behaviour in the tested temperature range, see Fig. 8-19.

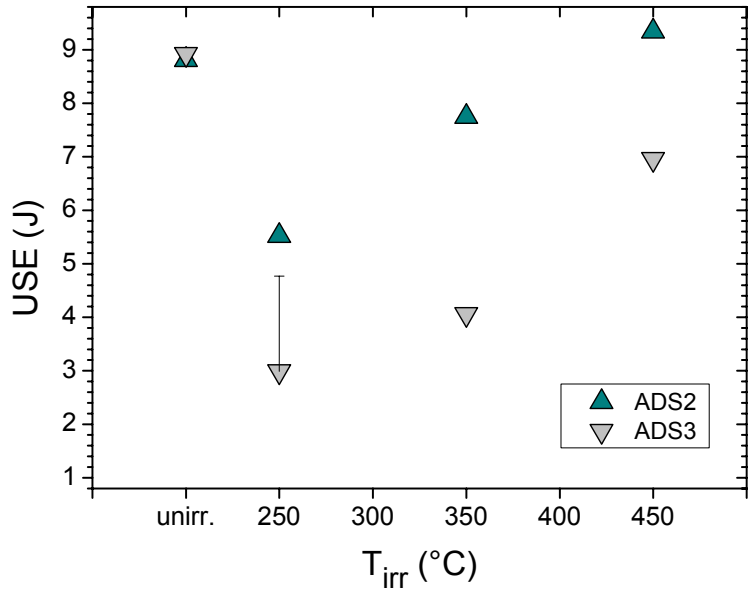

Fig. 3-9 Upper shelf energy vs. irradiation temperature for doped EUROFER steels. The error bar indicates uncertainty in the USE of ADS3 at T_{irr} =250°C.

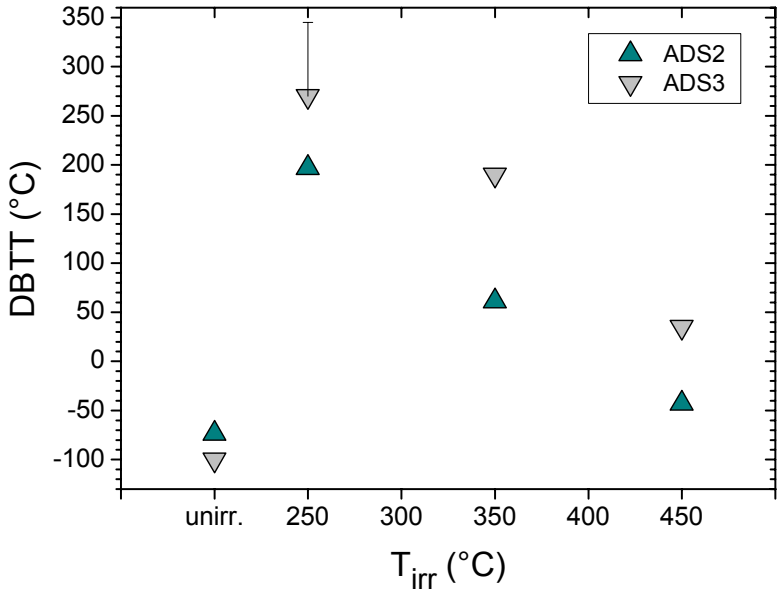

Fig. 3-10 Ductile-to-brittle transition temperature vs. irradiation temperature for ADS steels. The error bar indicates uncertainty in the DBTT of ADS3 at T_{irr} =250°C.

Fig. 3-10 shows the DBTT as a function of irradiation temperature (T_{irr}) for ADS2 and ADS3 steels. At all irradiation temperatures ADS3 shows basically larger DBTT than ADS2. Uncertainty in DBTT at T_{irr} =250°C for ADS3 originates in the uncertainty in the USE shown in Fig. 3-9.

Fig. 3-11 shows the LTUS as a function of irradiation temperature (T_{irr}) for ADS2 and ADS3. LTUS shows essentially the same behaviour as DBTT being mostly influenced by neutron irradiation at T_{irr} =250°C.

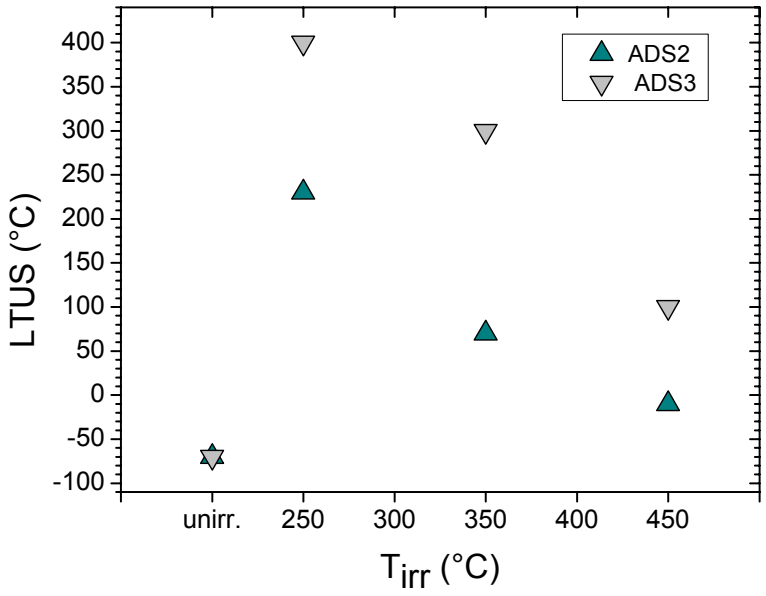

Fig. 3-11 Lowest temperature in the upper shelf vs. irradiation temperature for ADS2 and ADS3. The result in the unirradiated condition is also included.

Fig. 3-12 shows dynamic yield stress as a function of irradiation temperature (T_{irr}) for ADS2 and ADS3 steels. In the unirradiated condition both steels show comparable σ_{RT} and σ_{100} values. In the 16.3dpa/450°C irradiation condition, however, the steel doped 83 wppm ^{10}B shows stronger hardening than the 82 wppm nat. B doped steel correlating with stronger embrittlement in the former case.

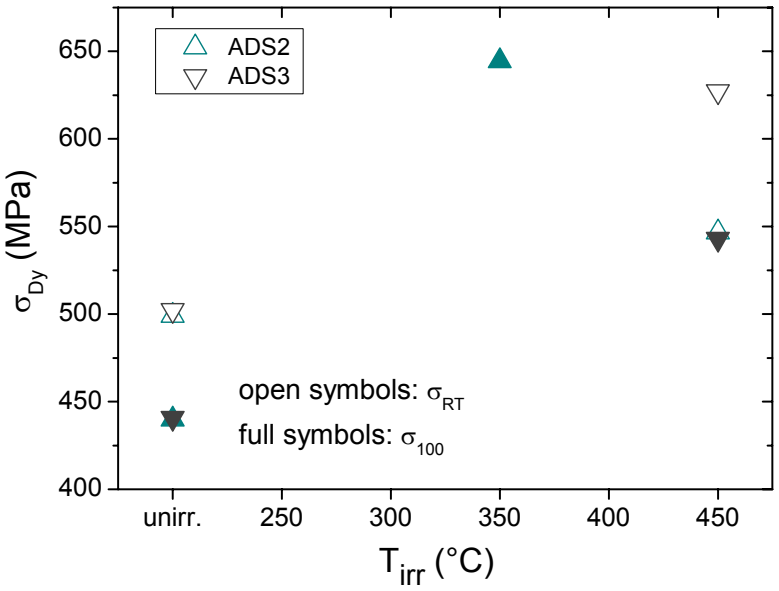

Fig. 3-12 Dynamic yield stress vs. irradiation temperature for ADS2 and ADS3; open symbols: σ_{RT}, full symbols σ_{100}. For comparison, the results in the unirradiated condition are also included.

4 Analyses of Irradiation influence

4.1 RAFM steels

4.1.1 Reduction of Upper Shelf Energy

Fig. 4-1 shows neutron irradiation induced reduction of the upper shelf energy vs. irradiation temperature (T_{irr}) for RAFM steels. Neutron irradiation at T_{irr} =300°C has the largest influence on the impact toughness of EUROFER97 ANL, where the USE is reduced by 30%. While at T_{irr} =250°C EUROFER97 WB shows slightly better irradiation resistance than EUROFER97 WB, at T_{irr} =350°C and at T_{irr} =450°C both variants of EUROFER steel show comparable impact toughness degradation. At T_{irr} =300°C the reduction in impact toughness for F82H-MOD is comparable to that of EUROFER97, whereas OPTIFER-Ia shows slightly better impact performance. At T_{irr} =400°C F82H-MOD and GA3X steels show the best impact toughness among all RAFM steels.

As estimated in Table 2-3 radiation dose received by 300°C drum is about 14.8 dpa in comparison to 13.6 dpa received by 250°C drum. This circumstance has to be taken into account while comparing the results at 250 and 300°C target temperatures.

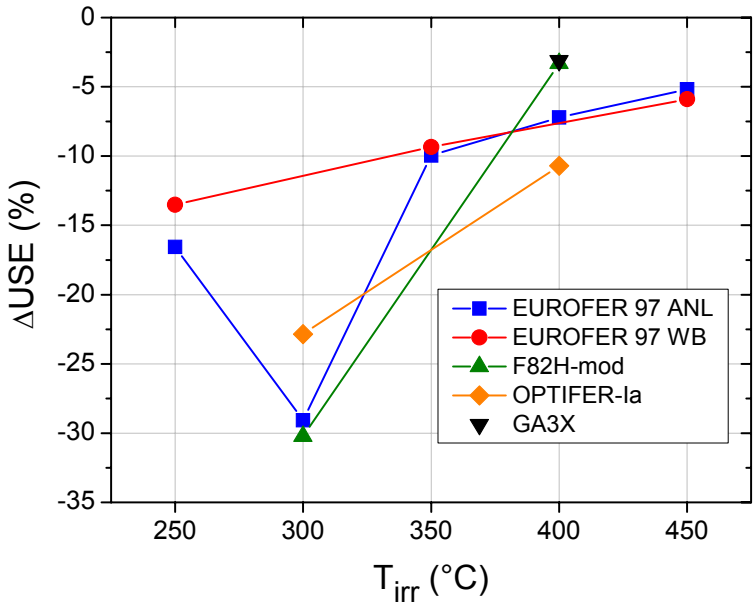

Fig. 4-1 Reduction of USE vs. irradiation temperature for RAFM steels.

4.1.2 Shift of DBTT

Fig. 4-2 shows neutron irradiation induced shift of the DBTT vs. irradiation temperature (T_{irr}) for RAFM steels. Strong embrittlement is observed for all RAFM steels below T_{irr} ≤300°C. At T_{irr} =250°C EUROFER97 WB shows superior embrittlement behaviour compared to EUROFER97 ANL, whereas at T_{irr}=350°C and at T_{irr} =450°C the embrittlement behaviour of both steels are comparable. At T_{irr} =300°C all irradiated RAFM steels show similar embrittlement which is comparable to that of EUROFER97 ANL at T_{irr} =250°C. Above T_{irr} ≥350°C all RAFM steels show moderate embrittlement. The GA3X steel shows a negative shift in DBTT at T_{irr} = 400°C – a behaviour already observed in [4] in the 0.8dpa/450°C irradiation condition.

4.1.3 Change of Dynamic Yield Stress

Fig. 4-3 shows neutron irradiation induced change of the dynamic yield stress vs. irradiation temperature (T_{irr}) for RAFM steels for two test temperature bins at room temperature (σ_{RT}) and at 100°C (σ_{100}). Strong hardening for all RAFM below T_{irr} ≤300°C correlates with strong embrittlement observed in Fig. 4-2. At T_{irr} =250°C and at T_{irr} =450°C both variants of the EUROFER97 steel show similar hardening, whereas at T_{irr} = 350°C EUROFER97 ANL shows superior hardening behaviour. At T_{irr} =300°C EUROFER97 ANL shows the lowest hardening among all RAFM steels. At T_{irr} ≥400°C all RAFM steels, with exception of OPTIFER-Ia, show slight hardening or even slight softening in a good correlation with low embrittlement at corresponding irradiation temperatures.

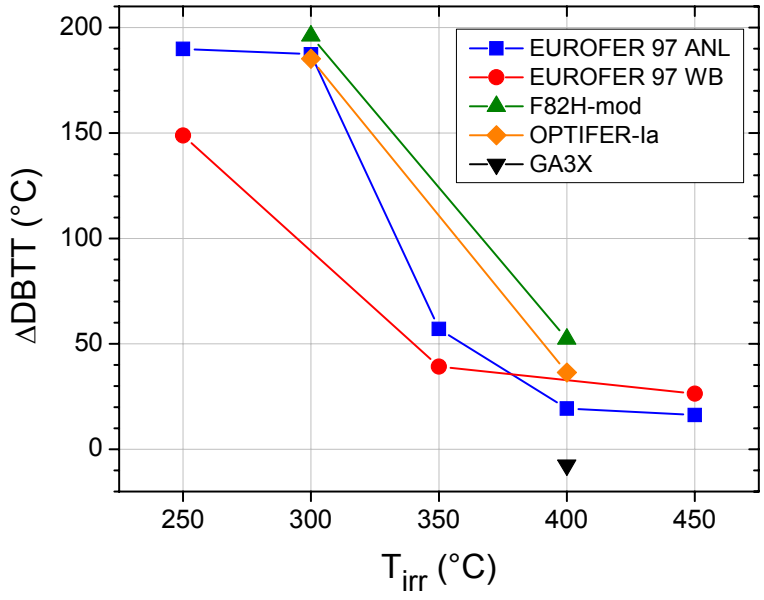

Fig. 4-2 Shift of DBTT vs. irradiation temperature for RAFM steels.

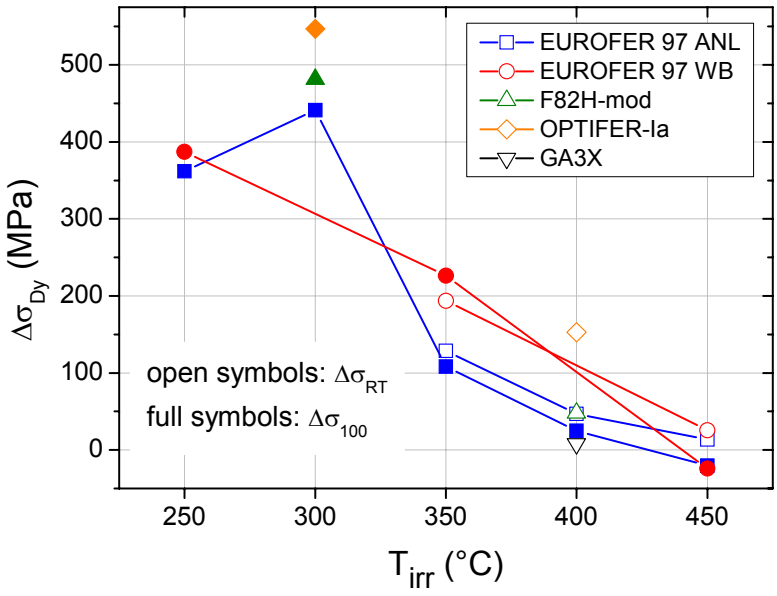

Fig. 4-3 Change of σ_{Dy} vs. irradiation temperature for RAFM steels.

4.2 ODS EUROFER

4.2.1 Change of Upper Shelf Energy

Fig. 4-4 shows neutron irradiation induced change of the upper shelf energy vs. irradiation temperature (T_{irr}) for hipped ODS EUROFER. At T_{irr} ≤350°C ODS EUROFER shows positive shift in the USE, indicating not optimized impact toughness in the unirradiated condition. At T_{irr} =450°C the USE is decreased by ~ 5% similar to the behaviour observed in Fig. 4-1 for EUROFER97.

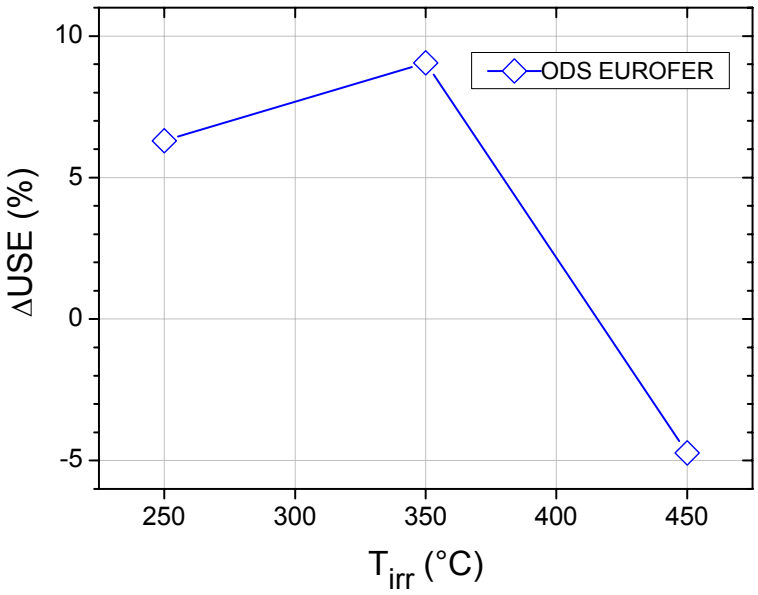

Fig. 4-4 Change of the upper shelf energy vs. irradiation temperature for hipped ODS EUROFER.

4.2.2 Shift of DBTT

Fig. 4-5 shows neutron irradiation induced shift of the DBTT vs. irradiation temperature (T_{irr}) for hipped ODS EUROFER. The shift in DBTT at T_{irr} =250°C is comparable to that of base EUROFER97 ANL steel. At T_{irr} =350°C, however, ODS EUROFER shows stronger embrittlement than EUROFER97 ANL. The embrittlement at T_{irr} =450°C is comparable to that of EUROFER97 steels.

4.2.3 Change of Dynamic Yield Stress

Fig. 4-6 shows neutron irradiation induced change of the dynamic yield stress vs. irradiation temperature (T_{irr}) for hipped ODS EUROFER. Due to the reasons mentioned in section 3.2 the hardening behaviour is summarised at 350°C testing temperature. The hardening is mostly pronounced at T_{irr} =350°C in contrast to the observations on base RAFM steels in Fig.

4-3, where the hardening is highest at low (T_{irr} ≤300°C) irradiation temperatures. Similar to base EUROFER97 steel, ODS EUROFER shows softening at T_{irr} =450°C.

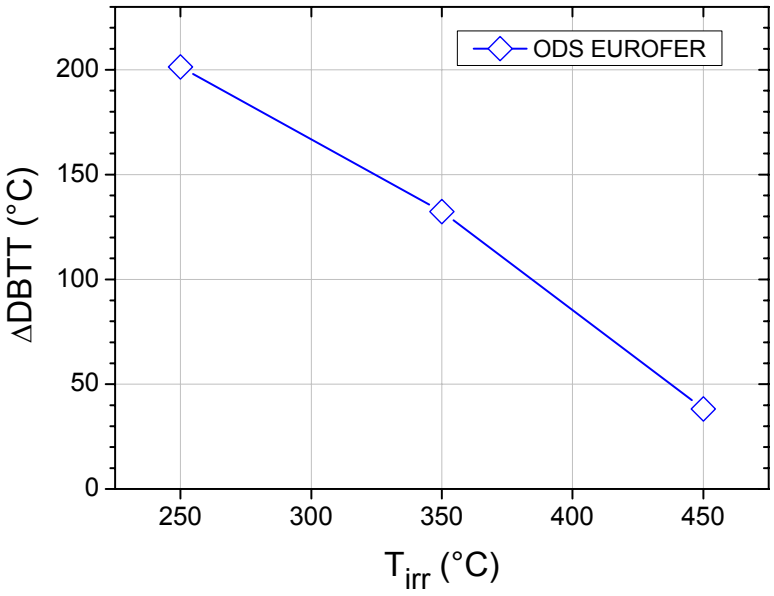

Fig. 4-5 Shift of DBTT vs. irradiation temperature for hipped ODS EUROFER.

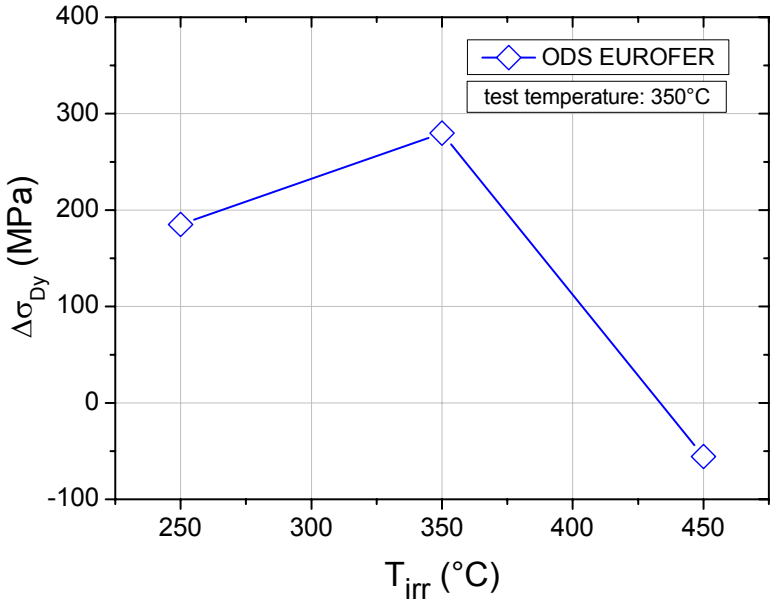

Fig. 4-6 Change of σ_{Dy} vs. irradiation temperature for hipped ODS EUROFER.

4.3 Boron Doped Steels

4.3.1 Change of Upper Shelf Energy

Fig. 4-7 shows neutron irradiation induced change of the upper shelf energy vs. irradiation temperature (T_{irr}) for ADS2 and ADS3. For comparative purpose the results on the EUROFER97 steel is also included. At T_{irr} =250°C boron doped steels exhibit large reduction in the USE, which is more pronounced for ^{10}B isotope doped steel. At T_{irr} =350°C decrease in the impact toughness for ADS2 is comparable to that for EUROFER97 WB. The ^{10}B isotope doped steel in contrast shows nearly 55% decrease of the USE. At T_{irr} =450°C ADS2 shows positive shift in USE, whereas, the USE of ADS3 is still degraded by more than 20%.

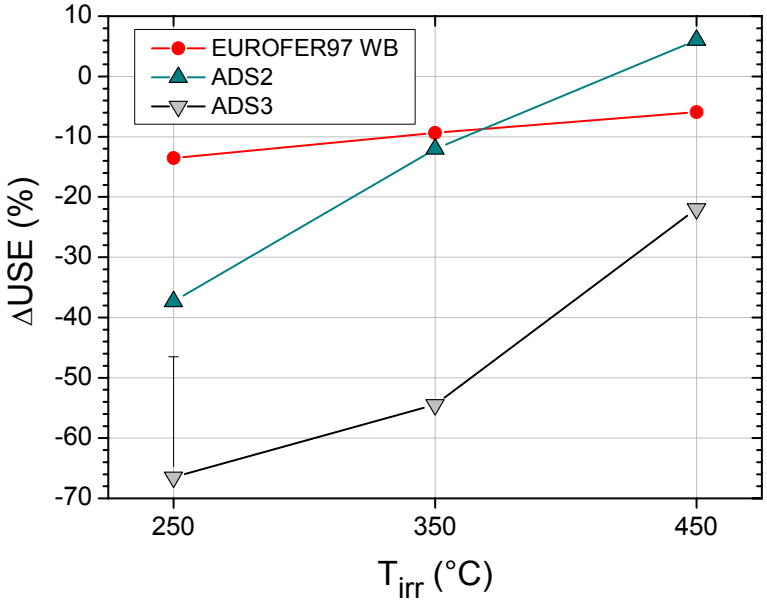

Fig. 4-7 Change of the upper shelf energy vs. irradiation temperature for Boron doped steels and EUROFER97 WB. The error bar indicates uncertainty in the USE of ADS3 at T_{irr} =250°C.

4.3.2 Shift of DBTT

Fig. 4-8 shows neutron irradiation induced shift of the DBTT vs. irradiation temperature (T_{irr}) for ADS2 and ADS3. For comparative purpose the results on the EUROFER97 WB steel is also included. Compared to EUROFER97 WB, ADS2 shows additional embrittlement at T_{irr} ≤350°C. The ^{10}B isotope doped steel (ADS3) exhibits the largest embrittlement at all irradiation temperatures.

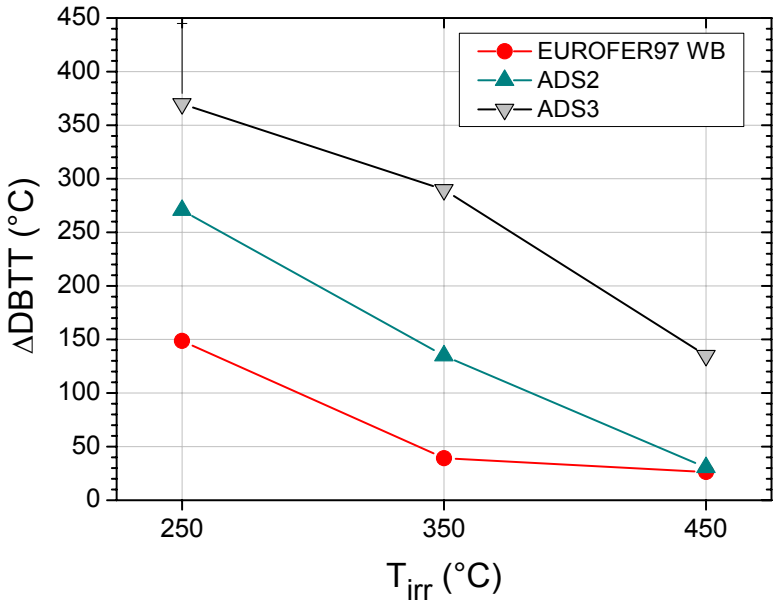

Fig. 4-8 Shift of DBTT vs. irradiation temperature for boron doped steels and EUROFER97 WB. The error bar indicates uncertainty in the DBTT of ADS3 at T_{irr} =250°C.

4.3.3 Change of Dynamic Yield Stress

Fig. 4-9 shows neutron irradiation induced change of the dynamic yield stress vs. irradiation temperature (T_{irr}) for ADS2 and ADS3 for two test temperature bins at room temperature (σ_{RT}) and at 100°C (σ_{100}). For comparative purpose the corresponding results on the EUROFER97 WB are also included. Hardening of ADS2 is comparable to that of the corresponding base metal. ADS3 doped with ^{10}B isotope, however, shows additional hardening at T_{irr} =450°C compared to EUROFER97 WB.

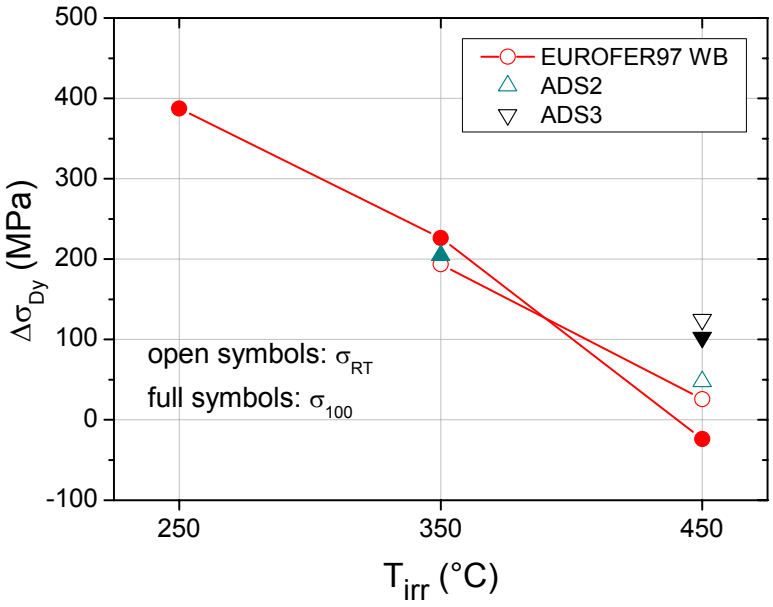

Fig. 4-9 Change of the dynamic yield stress vs. irradiation temperature for ADS2, ADS3 and EUROFER97 WB steels for two test temperature bins at room temperature (σ_{RT}) and at 100°C (σ_{100}).

5 Discussion

5.1 RAFM Steels

5.1.1 Discussion of Individual Steels

Impact properties of EUROFER97 ANL are mostly influenced by neutron irradiation at low irradiation temperatures T_{irr} ≤300°C [16],[17]. Although material embrittlement (ΔDBTT) is nearly identical for 250°C and 300°C irradiation conditions, the impact toughness (USE) is mostly degraded at T_{irr} =300°C. This observation can be partly ascribed to different average damage doses received by individual drums as summarised in Table 2-3. The irradiation induced hardening ($\Delta\sigma_{Dy}$) correlates with the toughness reduction being largest at T_{irr} =300°C. The influence of the neutron irradiation on the impact properties of EUROFER97 ANL is substantially reduced at T_{irr} =350°C and nearly vanishes above T_{irr} ≥400°C.

Heat treatment of EUROFER97 at higher austenitizing temperature (T_{Au} =1040°C) improved steel irradiation resistance at T_{irr} ≤350°C. Indeed, the irradiation induced degradation of impact toughness (ΔUSE) as well as embrittlement (ΔDBTT) were substantially reduced compared to base EUROFER97 ANL steel (T_{Au} =980°C). Although EUROFER97 WB showed superior embrittlement behaviour than EUROFER97 ANL at T_{irr} =350°C, the latter exhibited less pronounced hardening. At T_{irr} =450°C both steels showed similarly good irradiation resistance.

Irradiation resistance of Japanese reference RAFM steel F82H-mod is comparable to that of EUROFER97 ANL [16],[17]. The embrittlement behaviour of F82H-mod, however, was somewhat worse than that of EUROFER97 ANL and showed large impact energy scattering in the ductile-to-brittle transition region at T_{irr} =300°C and larger embrittlement (ΔDBTT) at T_{irr} =400°C.

The reference steel OPTIFER-Ia showed the best impact toughness both in the unirradiated and irradiated conditions. Irradiation induced embrittlement (ΔDBTT) is comparable to that of EUROFER97 ANL at T_{irr}=300°C and lies between EUROFER97 ANL and F82H-mod at T_{irr} =400°C.

The reference steels GA3X showed impact toughness (USE) and DBTT comparable to that of EUROFER97 ANL at T_{irr} =400°C. The irradiation induced hardening ($\Delta\sigma_{Dy}$) was lowest among all investigated RAFM steels.

No simple correlation can be drawn between the grain size and upper shelf energy. The finest grain structure of OPTIFER-Ia, as inferred from the Table 8-2, however might be an explanation for the superior USE of OPTIFER-Ia in unirradiated and irradiated conditions.

For boron contents below 62 wppm, the influence of boron to helium transformation on embrittlement can not be resolved for 16.3 dpa irradiated RAFM steels in clear contrast to higher boron contents and lower irradiation doses (up to 2.4 dpa), where ^{10}B burn-up indeed contributed to the embrittlement to a large extent [9],[7].

The influence of the neutron irradiation on the LTUS is essentially similar to that on the DBTT for all investigated RAFM steels.

5.1.2 Embrittlement Behaviour of EUROFER97

Irradiation dose dependence of the DBTT for EUROFER97 obtained recently in the literature [18],[19] is plotted in Fig. 5-1 to compare with the results obtained in the current irradiation programme. A progressive material embrittlement with the irradiation dose is seen for T_{irr}=300-330°C. Relatively large DBTT value for 8.9dpa/300°C irradiated condition may be explained by large uncertainty in the DBTT due to large impact energy scattering. Good agreement between the results obtained for 15dpa/330°C irradiated steel in [19] and in the present work is remarkable.

The shift in DBTT vs. irradiation dose is plotted in Fig. 5-2 for EUROFER97 steel irradiated between 300 and 330°C [16]. For comparison, the data reported in [18] and in [19] are presented as well. Large data scattering at low and intermediate doses prevents a quantitative analysis of the embrittlement trend. Furthermore, it has to be noted that the dose of 32 dpa was achieved at 330°C [19]. As shown in the present work, the shift in DBTT is very sensitive to the irradiation temperature between 300 and 350°C and substantially decreases at 350°C. Having all these facts in mind, no unambiguous estimation of embrittlement saturation is

possible on the basis of the data available. Consequently, embrittlement data at higher irradiation doses are indispensable for a structure material qualification.

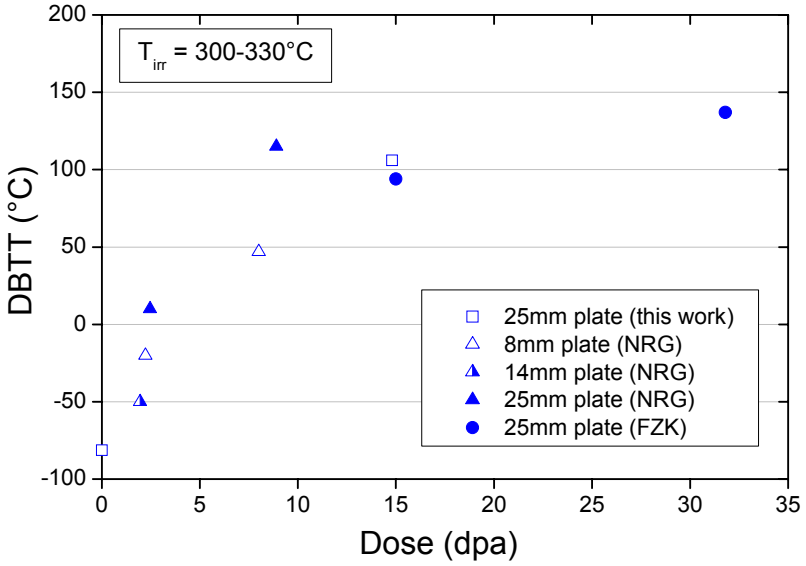

Fig. 5-1 DBTT vs. irradiation dose for EUROFER97. The triangles (T_{irr} =300°C) are from [18] and the circles (T_{irr} =330°C) are from [19].

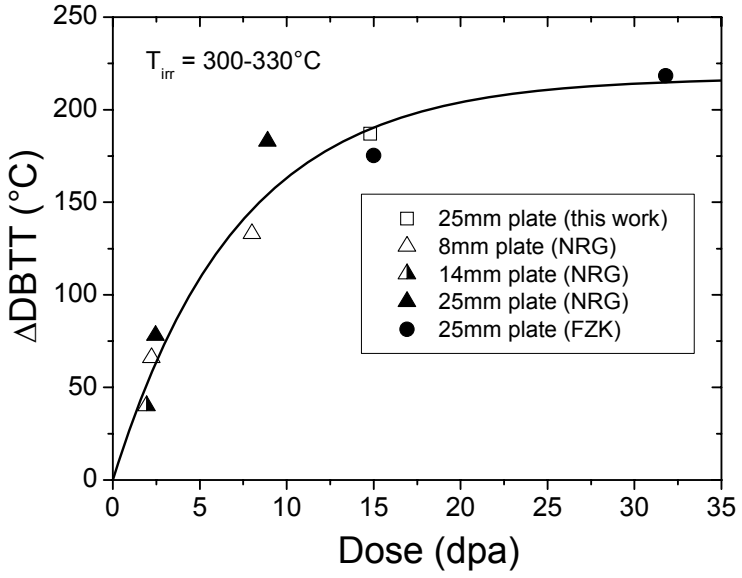

Fig. 5-2 Shift in DBTT vs. irradiation dose for EUROFER97. The triangles (T_{irr} =300°C) are from [18] and the circles (T_{irr} =330°C) are from [19]. The line is the $\Delta DBTT=\Delta DBTT_{sat}(1-\exp(-Dose/Dose_0))$ fit for the presented data, with $\Delta DBTT_{sat}$ and $Dose_0$ as fitting parameters. The weighted least square method (weighting factors $\propto$ Dose) resulted in $\Delta DBTT_{sat}$=217.5°C and $Dose_0$=7.2 dpa.

5.1.3 Hardening vs. Embrittlement Behaviour

The hardening vs. embrittlement behaviour was quantified in terms of the hardening shift coefficient C defined as $C=\Delta DBTT/\Delta\sigma$ [20]. Fig. 5-3 displays this parameter for two test temperature bins at room temperature (C_{RT}) and at 100-120°C (C_{100}) [16]. At $T_{irr}\leq$ 350°C, the coefficient C varies between $0.17\leq C\leq 0.53$ °C/MPa [16] in a good agreement with the analysis on 7-9%Cr RAFM steels yielding $C=0.38\pm0.18$ °C/MPa [20] and indicating that embrittlement is dominated by a hardening mechanism. The hardening shift coefficient C_{100} tends to increase at T_{irr}= 400°C. This suggests a non-hardening embrittlement (NHE) mechanism that primarily occurs under thermal aging conditions. Depending on the nature of the dominating NHE mechanism the coefficient C may become large, very small or even negative at $T_{irr}\geq$ 400°C in case of material softening [20].

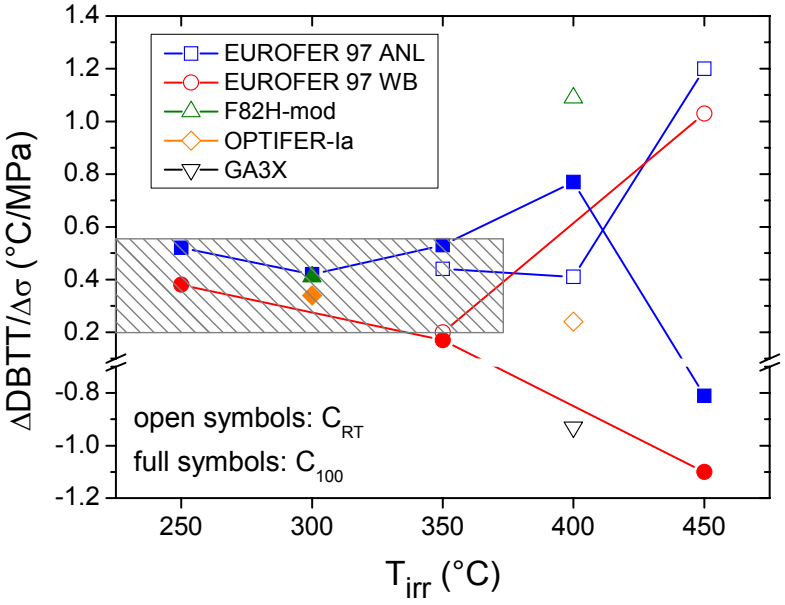

Fig. 5-3 Hardening shift coefficient C vs. irradiation temperature; open symbols: C_{RT}, full symbols C_{100}, see text for explanation. Dashed area indicates scattering band for $C=0.38\pm0.18$ °C/MPa from [20].

5.2 ODS EUROFER

Hipped ODS EUROFER with 0.5 wt.% Y_2O_3 showed not satisfying impact properties already in the unirradiated condition characterized by low USE =2.54 J and large DBTT = 135°C. Furthermore, the increase of USE for irradiation temperatures below $T_{irr}\leq$350°C indicates not optimized fabrication process. At low irradiation temperature (T_{irr} =250°C) neutron irradiation induced shift in DBTT is comparable to that of the base EUROFER steel. At higher irradiation temperatures, however, hipped ODS EUROFER shows larger embrittlement compared to base metal. Improvement of the impact properties will be main prerequisite for material qualification for future fusion reactors.

5.3 Boron Doped Steels

Boron doped steels show up as expected degraded neutron irradiation resistance compared to the EUROFER97 steel [21]. Comparative studies of EUROFER97 steels doped with 82 wppm natural boron (0.2 ^{10}B+0.8 ^{11}B) and with 83 wppm separated ^{10}B isotope proved ^{10}B doped steel to be more susceptible to irradiation embrittlement. The ^{10}B isotope is a strong thermal neutron absorber and transforms to helium and lithium already at moderate neutron fluxes by ^{10}B(n,α) ^{7}Li reactions. Helium bubbles formed in the steel matrix or at grain boundaries can produce severe embrittlement in the irradiated materials. It is noteworthy, that the generated helium amount of 432 appm [14] for examined ^{10}B content of 83 wppm is quite relevant for the future fusion reactor of DEMO type with helium to damage dose ratios of 11-13 appm/dpa and with the expected accumulated damage dose of 100-150 dpa. However, the results of boron-to-helium transformation experiments can not be unambiguously applied to fusion relevant conditions. During fission reactor irradiation, all the boron is quickly transformed into helium (the burn-up constant for a decrease of ^{10}B amount to 37% of its initial value is τ =0.34dpa [9]), which differs from what happens in a fusion reactor, where helium forms simultaneously and more gradually with the displacement damage. This may lead to the different swelling behaviour for boron doped and fusion experiments.

Boron mediated enhancement of irradiation induced DBTT shift (i.e. extra DBTT shift in comparison to the EUROFER97 steel), as shown in Fig. 4-8, is relatively high at irradiation temperatures below T_{irr} ≤350°C and remarkably reduces at T_{irr} =450°C. This behaviour qualitatively correlates with the irradiation induced hardening that is relatively large below T_{irr} ≤350°C and reduces at T_{irr} =450°C as shown e.g. in Fig. 8-18. At T_{irr}=250°C the hardening shift coefficient for ADS2 C_{200}=0.57 °C/MPa compares to that of EUROFER97 C_{200}=0.57 °C/MPa indicating that the extra embrittlement of ADS2 is mainly related to extra hardening due to 84 appm helium production. For ADS3, however, C_{250}=0.74 °C/MPa is much larger than the corresponding value for EUROFER97 C_{250}=0.56 °C/MPa indicating the existence of additional embrittlement mechanisms beyond to the helium induced hardening. At T_{irr}=450°C the hardening shift coefficient C_{RT} was 0.64 and 1.08 °C/MPa for ADS2 and ADS3 steels, respectively, indicating non-hardening-helium-embrittlement being more pronounced for ADS3 steel (due to larger helium amount produced).

Irradiation induced DBTT shift of EUROFER97 steel doped with 1120 wppm separated ^{10}B isotope could not be quantified due to large embrittlement found in the investigated temperature range, see Fig. 8-19. Such a large embrittlement, however, should not be only related to helium generation but also to the degraded impact properties in the unirradiated condition.

6 Conclusion

European reference RAFM steel EUROFER97 irradiated up to 16.3 dpa (average) at 250, 300, 350, 400 and 450°C showed embrittlement behaviour and hardening comparable to that of the best reference RAFM steels. At T_{irr}=300°C, the DBTT and the dynamic yield stress of EUROFER97 are comparable to those of OPTIFER-Ia. The latter showed the best impact

toughness at T_{irr}=300 °C. The embrittlement behaviour of reference material F82H-mod at T_{irr}=300 °C is somewhat worse than that of EUROFER97 ANL, showing large impact energy scattering in the ductile-to-brittle transition region. At T_{irr}=400 °C, the embrittlement behaviour of EUROFER97 is superior to that of OPTIFER-Ia and F82H mod, though the DBTTs of these materials remain below -30 °C. Heat treatment of the as-delivered EUROFER97 plate led to the reduction of the embrittlement at low irradiation temperatures. The hardening shift coefficient *C* varied between 0.17≤ *C*≤ 0.53 °C/MPa at T_{irr}≤ 350 °C in a good agreement with literature [20], indicating hardening embrittlement mechanism. At T_{irr}≥400 °C large scattering of the coefficient *C* indicates non-hardening embrittlement mechanism.

The influence of boron-to-helium transformation on embrittlement cannot be resolved for 16.3 dpa irradiated RAFM steels with boron contents between 4 and 62 wppm. Boron doped steels with boron concentrations between 83 and 1120 wppm show progressive embrittlement and reduction of toughness with produced He amount up to 5580 appm. At T_{irr} =250 °C He induced embrittlement is of hardening nature for low helium contents up to 84 appm. Larger helium concentrations lead to non-hardening embrittlement mechanisms beyond that of hardening embrittlement. At higher irradiation temperatures helium tends to increasingly contribute to non-hardening embrittlement mechanisms.

The state of the art of the structure materials may be successfully combined with the special fusion reactor design with operating temperature range for the first wall and blanket modules between 350 and 450 °C.

7 References

[1] M. Rieth, B. Dafferner, C. Wassilew, Der Einfluss von Wärmebehandlung und Neutronenbestrahlung auf die Kerbschlageigenschaften des martensitischen 10,6% Cr-Stahls MANET-I, Institut für Materialforschung, Kernforschungszentrum Karlsruhe, KfK-Bericht 5243, September 1993.

[2] M. Rieth, B. Dafferner, H. Ries, O. Romer, Bestrahlungsprogramm MANITU: Ergebnisse der Kerbschlagbiegeversuche mit den bis 0,8 dpa bestrahlten Werkstoffen der ersten Bestrahlungsphase, Forschungszentrum Karlsruhe, FZKA 5619, Sept. 1995.

[3] M. Rieth, B. Dafferner, H. Ries, O. Romer, Bestrahlungsprogramm MANITU: Ergebnisse der Kerbschlagbiegeversuche mit den bis 0,2 dpa bestrahlten Werkstoffen, Forschungszentrum Karlsruhe, FZKA 5750, April 1997.

[4] H.-C. Schneider, M. Rieth, B. Dafferner, H. Ries, O. Romer, Bestrahlungsprogramm MANITU: Ergebnisse der Kerbschlagbiegeversuche mit den bis 0,8 dpa bestrahlten Werkstoffen der zweiten Bestrahlungsphase, Forschungszentrum Karlsruhe, FZKA 6519, September 2000.

[5] H.-C. Schneider, B. Dafferner, H. Ries, O. Romer, Bestrahlungsprogramm MANITU: Ergebnisse der Kerbschlagbiegeversuche mit den bis 2,4 dpa bestrahlten Werkstof-

fen, Forschungszentrum Karlsruhe, FZKA 6605, Mai 2001.

[6] H.-C. Schneider, B. Dafferner, J. Aktaa, Embrittlement behaviour of low-activation alloys with reduced boron content after neutron irradiation, J. Nucl. Mater. 321 (2003) 135-140.

[7] H.-C. Schneider, B. Dafferner, H. Ries, S. Lautensack, O. Romer, Bestrahlungsprogramm HFR Phase Ib: Ergebnisse der Kerbschlagbiegeversuche mit den bis 2,4 dpa bestrahlten Werkstoffen, Forschungszentrum Karlsruhe, FZKA 6976, April 2004.

[8] R. Lindau, A. Moeslang, M. Schirra, P. Schlossmacher, M. Klimenkov, Mechanical and microstructural properties of a hipped RAFM ODS-steel, Journal of Nuclear Materials 307-311 (2002) 769-772.

[9] M. Rieth, B. Dafferner, H.D. Röhrig, Embrittlement behaviour of different international low activation alloys after neutron irradiation, J. Nucl. Mater. 258-263 (1998) 1147.

[10] H.-C. Schneider, unpublished report, December 2002.

[11] P. Graf et al., Der Einfluss von Bor auf die Gefügeeigenschaften von martensitischen 9%-Chromstählen, P. Portella [Hrsg.], Fortschritte in der Metallographie: Vortragstexte der 37.Metallographie-Tagung, Berlin, 17.-19. September 2003; Frankfurt: Werkstoff-Informationsgesellschaft mbH, 2004 S.71-76 (Sonderbände der Praktischen Metallographie ; 35).

[12] J. Ahlf, A. Zurita, High Flux Reactor (HFR) Petten - Characteristics of the Installation and the Irradiation Facilities, Nuclear Science and Technology, EUR 15151 EN, 1993.

[13] H. Lohner, Sample Holder for Irradiation of Miniaturised Stee Specimens Simultaneously at Different Temperatures, Project 329-01, Irradiation Report, Technical Memorandum HFR/04/4779.

[14] D. J. Ketema, J.I. Wolters, Sample Holder for Irradiation of Miniaturised Steel Specimens Simultaneously at Different Temperatures, SPICE-T (330-09), Neutron Metrology, NRG, Petten, 21400/05.65267/C.

[15] J.M. Alexander, T.J. Komoly, On the yielding of a rigid/plastic bar with an IZOD notch, J. Mech. Phys. Solids, 10 (1962) 265-275.

[16] E. Gaganidze, H.-C. Schneider, B. Dafferner, J. Aktaa, High-dose neutron irradiation embrittlement of RAFM steels, J. Nucl. Mater. 355 (2006) 83.

[17] E. Gaganidze, H.-C. Schneider, B. Dafferner, J. Aktaa, Embrittlement behavior of neutron irradiated RAFM steels, J. Nucl. Mater. 367-370 (2007) 81.

[18] J. Rensman, E. Lucon, J. Boskeljon, J. van Hoepen, R. den Boef, P. ten Pierick, Irradiation resistance of Eurofer97 at 300°C up to 10dpa, J. Nucl. Mater. 329-333 (2004)

1113-1116; J. Rensman, NRG Irradiation Testing: Report on 300°C and 60°C Irradiated RAFM Steels, Final Report for subtask TW2-TTMS-001a D06 and TW2-TTMS-001b D12, Petten, August 2005, 20023/05.68497/P.

[19] C. Petersen, A. Povstyanko, V. Prokhorov, A. Fedoseev, O. Makarov, B. Dafferner, Impact property degradation of ferritic/martensitic steels after the fast reactor irradiation 'ARBOR 1', J. Nucl. Mater. 367–370 (2007) 544.

[20] T. Yamamoto, G. R. Odette, H. Kishimoto, J.-W. Rensman, P. Miao, J. Nucl. Mater. 356 (2006) 27; T. Yamamoto, H. Kishimoto, G.R. Odette, Fusion Materials Semiannual Report 7/1 to 12/31/2003 DOE/ER-313/34; G.R. Odette, T. Yamamoto, H.J. Rathbun, M.Y. He, M.L. Hribernik, J.W. Rensman, J. Nucl. Mater. 323 (2003) 313.

[21] E. Gaganidze, B. Dafferner and J. Aktaa, Neutron Irradiation Resistance of RAFM Steels, Proceedings of 2006 MRS Fall Meeting, Nov 27 - Dec. 1, Boston, USA, MRS Symp. Proc.; 981E, Electronic-Only Publication.

8 Appendix

8.1 Material Chemical Composition

		Hipped Steel	Boron doped EUROFER steels			Reference RAFM steels			10-11% Cr-NiMoVNb
MATERIAL	**EUROFER 97**	**EUROFER ODS HIP 0.5%Y2O3**	**OPTIFER-VIII (ADS2)**	**ADS3**	**ADS4**	**GA3X**	**F82H mod.**	**OPTIFERIa**	**MANET-I**
Heat	83697	0958/3-2	806	826	825		9741	664	53645
Cr	8.91	9.40	9.31	8.80	9.0	9.17	7.7	9.33	10.8
W	1.08	1.10	1.27	1.125	1.06	2.12	2.04	0.965	
Mn	0.48	0.418	0.602	0.395	0.38	0.042	0.16	0.50	0.76
V	0.2	0.185	0.19	0.193	0.197	0.314	0.16	0.26	0.2
Ta	0.14	0.080	0.055	0.088	0.08	0.011	0.009	0.066	
C	0.12	0.072	0.109	0.095	0.100	0.159	0.09	0.10	0.14
Si	0.04	0.115	0.020	0.031	0.03		0.11	0.06	0.37
P	0.005	<0.04	0.0035	0.0024	0.001		0.002	0.0046	0.005
S	0.004	0.0036	0.0030	0.003	0.0025		0.002	0.005	0.004
Ni	0.02	0.067	0.005	0.008	0.006	0.021	0.021	0.005	0.92
Mo	<0.001	0.004	0.002	0.046	0.028	0.0077	0.003	0.005	0.77
Nb	0.0017	<0.0005		0.005	0.002	0.011	0.0101	0.009	0.16
Al	0.009	0.0051	0.001	0.004	0.004	0.015	0.0016	0.008	0.054
B	0.001	<0.005	0.0082 ($^{10}B+^{11}B$)	0.0083 (^{10}B)	0.112 (^{10}B)		0.0004	0.0062	0.0085
N	0.02	0.029	0.021	0.028	0.0255	0.0018	0.008	0.0153	0.02
O	0.0008	0.171	0.013	0.0045	0.0037				
Co	0.006	0.0121				0.003	0.0037		0.01
Cu	0.0015	0.0151		0.006	0.005	0.0017	0.0063	0.035	0.015
Zr	<0.005						0.01		0.059
Ce			-					<0.001	
Ti	0.006	0.001		0.001	0.001	0.001	0.004	0.007	
As	<0.005							0.0093	
Sb	<0.005							<0.0002	
Sn	<0.005							0.0005	
Fe	balance	balance	balance	balance	balance	balance	balance	balance	balance

Table 8-1: Material chemical composition in wt.%

8.2 Heat Treatments and Selected Material Properties

	Heat treatment	Grain size (µm)	USE (J)	DBTT (°C)	Dynamic yield stress (MPa)
EUROFER97 ANL	980°C/0.5h + 760°C/1.5h	16	9.84	-81	543 @100°C
EUROFER97 WB	1040°C/0.5h + 760°C/1.5h	21.4	9.84	-91	486 @100°C
ODS EUROFER		2-8	2.54	135	773 @100°C
ADS2	1040°C/0.5h + 760°C/1.5h		8.81	-74	440 @100°C
ADS3	1040°C/0.5h + 760°C/1.5h		8.92	-100	441 @100°C
ADS4	1040°C/0.5h + 760°C/1.5h		5.5	-12	460 @100°C
GA3X	1000°C/1h + 700°C/2h	55±5	9.4	-58	650 @100°C
F82H-mod	950°C/0.5h + 750°C/2h	55	9.7	-86	446 @100°C
OPTIFER-Ia	900°C/0.5h + 780°C/2h	10	10.6	-81	482 @23°C
MANET-I	980°C/2h + 1075°C/0.5h + 750°C/2h	30±5	6.6	-30	670 @100°C

Table 8-2: Heat treatments and selected properties of unirradiated materials

8.3 Impact Testing: Results and Evaluation

8.3.1 EUROFER97 ANL

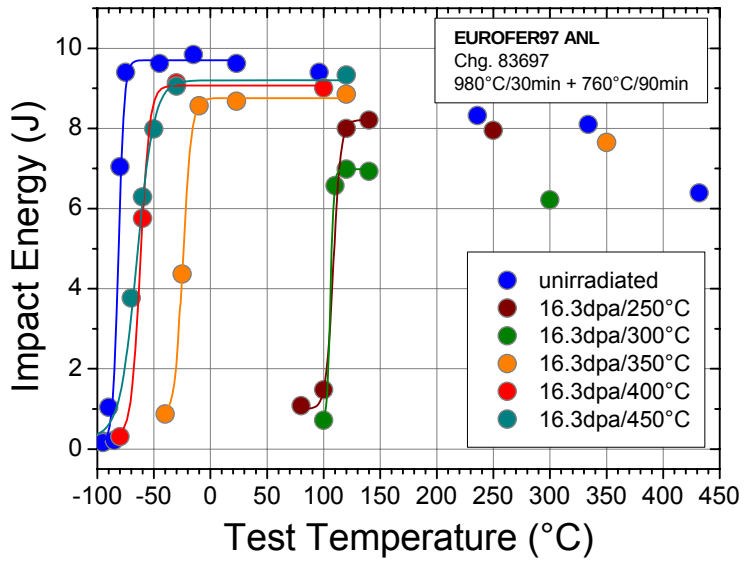

Fig. 8-1 Charpy impact energy vs. test temperature for unirradiated and 16.3 dpa (average) irradiated EUROFER97 ANL. The solid lines are fits according to Eq. (2-1).

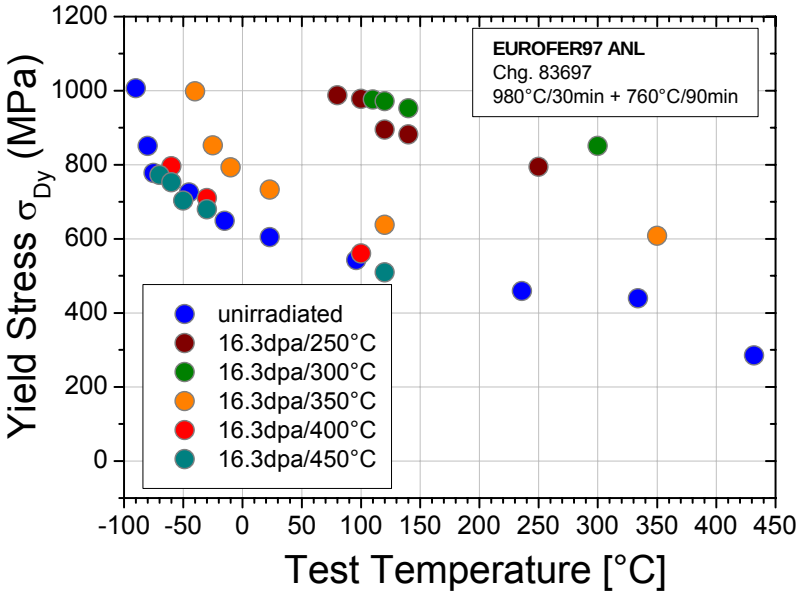

Fig. 8-2 Dynamic yield stress vs. test temperature for unirradiated and 16.3 dpa (average) irradiated EUROFER97 ANL.

Irradiation condition: unirradiated

Specimen	Test Temperature (°C)	Impact Energy (J)	Yield Stress (MPa)
UYA03	-95	0.19	-
UYA09	-95	0.16	-
UYA08	-90	1.04	1007
UYA07	-85	0.21	-
UYA06	-80	7.04	851
UYA02	-75	9.40	778
UYA11	-45	9.62	726
UYA10	-15	9.84	648
UYA01	23	9.62	604
UYA12	96	9.40	543
UYA13	236	8.32	459
UYA14	334	8.10	439
UYA15	432	6.39	284

Irradiation condition: 16.3dpa/250°C

Specimen	Test Temperature (°C)	Impact Energy (J)	Yield Stress (MPa)
YA03	80	1.08	988
YA04	100	1.48	1018
YA02	120	7.99	886
YA01	140	8.21	882
YA06	250	7.95	794

Irradiation condition: 16.3dpa/300°C

Specimen	Test Temperature (°C)	Impact Energy (J)	Yield Stress (MPa)
YA07	100	0.72	-
YA12	110	6.57	976
YA11	120	6.98	972
YA08	140	6.93	953
YA09	300	6.21	851

Irradiation condition: 16.3dpa/350°C

Specimen	Test Temperature (°C)	Impact Energy (J)	Yield Stress (MPa)
YA15	-40	0.87	998
YA16	-25	4.37	852
YA14	-10	8.56	793
YA13	23	8.68	733
YA18	120	8.86	638
YA17	350	7.65	608

Irradiation condition: 16.3dpa/400°C

Specimen	Test Temperature (°C)	Impact Energy (J)	Yield Stress (MPa)
YA23	-80	0.31	0
YA22	-60	5.76	796
YA21	-30	9.13	710
YA19	100	9.01	561

Irradiation condition: 16.3dpa/450°C

Specimen	Test Temperature (°C)	Impact Energy (J)	Yield Stress (MPa)
YA27	-70	3.77	772
YA26	-60	6.29	753
YA28	-50	7.98	704
YA25	-30	9.06	679
YA29	120	9.33	509

Evaluation:

Irradiation Condition	USE (J)	DBTT (°C)	LTUS (°C)	σ_{RT} (MPa)	σ_{100} (MPa)
unirradiated	9.84	-81	-75	604	541
16.3dpa/250°C	8.21	109	120	-	895
16.3dpa/300°C	6.98	106	110	-	972
16.3dpa/350°C	8.86	-24	-10	733	638
16.3dpa/400°C	9.13	-62	-30	651	566
16.3dpa/450°C	9.33	-65	-30	618	509

Irradiation Condition	ΔUSE (%)	ΔDBTT (°C)	$\Delta\sigma_{RT}$ (MPa)	$\Delta\sigma_{100}$ (MPa)
16.3dpa/250°C	-17	190	-	362
16.3dpa/300°C	-29	187	-	441
16.3dpa/350°C	-10	57	129	108
16.3dpa/400°C	-7	19	47	25
16.3dpa/450°C	-5	16	14	-20

8.3.2 EUROFER97 WB

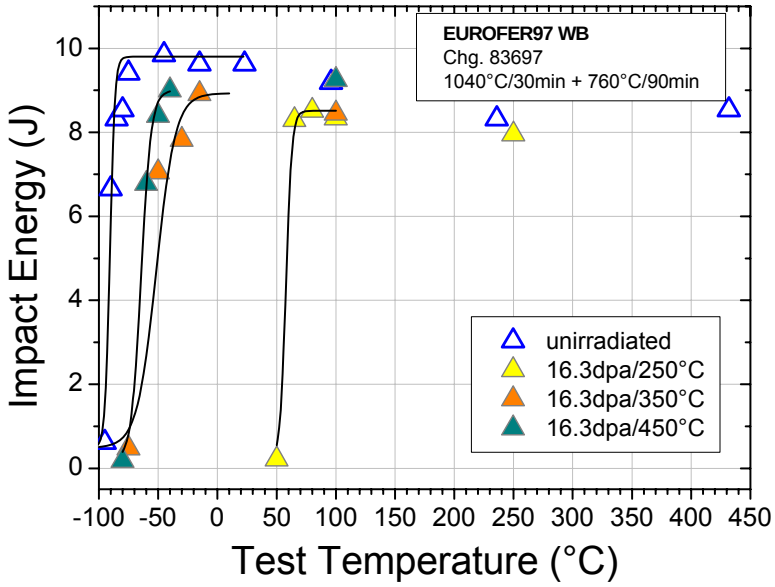

Fig. 8-3 Charpy impact energy vs. test temperature for unirradiated and 16.3 dpa (average) irradiated EUROFER97 WB. The solid lines are fits according to Eq. (2-1).

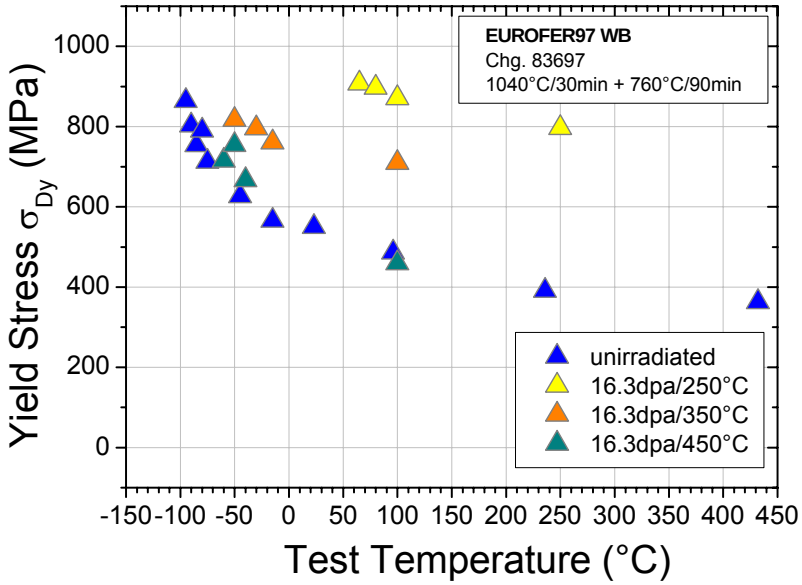

Fig. 8-4 Dynamic yield stress vs. test temperature for unirradiated and 16.3 dpa (average) irradiated EUROFER97 WB.

Irradiation condition: unirradiated

Specimen	Test Temperature (°C)	Impact Energy (J)	Yield Stress (MPa)
UYW10	-95	0.50	864
UYW09	-90	6.64	803
UYW08	-85	8.31	754
UYW07	-80	8.53	791
UYW02	-75	9.40	712
UYW12	-45	9.84	627
UYW11	-15	9.62	566
UYW01	23	9.62	550
UYW13	96	9.18	486
UYW14	236	8.32	391
UYW15	432	8.53	362

Irradiation condition: 16.3dpa/250°C

Specimen	Test Temperature (°C)	Impact Energy (J)	Yield Stress (MPa)
YW03	50	0.22	-
YW04	65	8.29	908
YW02	80	8.51	897
YW01	100	8.34	871
YW05	250	7.95	796

Irradiation condition: 16.3dpa/350°C

Specimen	Test Temperature (°C)	Impact Energy (J)	Yield Stress (MPa)
YW06	-75	0.48	1080
YW08	-50	7.05	817
YW07	-30	7.82	796
YW09	-15	8.91	761
YW10	100	8.45	710

Irradiation condition: 16.3dpa/450°C

Specimen	Test Temperature (°C)	Impact Energy (J)	Yield Stress (MPa)
YW15	-80	0.18	-
YW12	-60	6.77	716
YW13	-50	8.40	754
YW14	-40	9.00	667
YW11	100	9.25	460

Evaluation

Irradiation Condition	USE (J)	DBTT (°C)	LTUS (°C)	σ_{RT} (MPa)	σ_{100} (MPa)
unirradiated	9.84	-91	-75	550	484
16.3dpa/250°C	8.51	58	65	-	871
16.3dpa/350°C	8.92	-52	-15	744	710
16.3dpa/450°C	9.26	-64	-40	576	460

Irradiation Condition	ΔUSE (%)	ΔDBTT (°C)	$\Delta\sigma_{RT}$ (MPa)	$\Delta\sigma_{100}$ (MPa)
16.3dpa/250°C	-14	149	-	387
16.3dpa/350°C	-9	39	194	226
16.3dpa/450°C	-6	26	26	-24

8.3.3 F82H-MOD

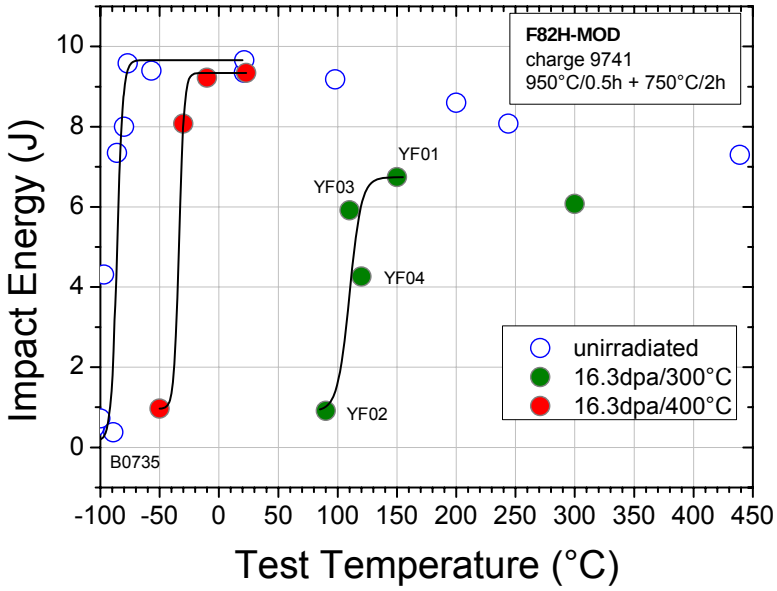

Fig. 8-5 Charpy impact energy vs. test temperature for unirradiated and 16.3 dpa (average) irradiated F82H-mod. The solid lines are fits according to Eq. (2-1).

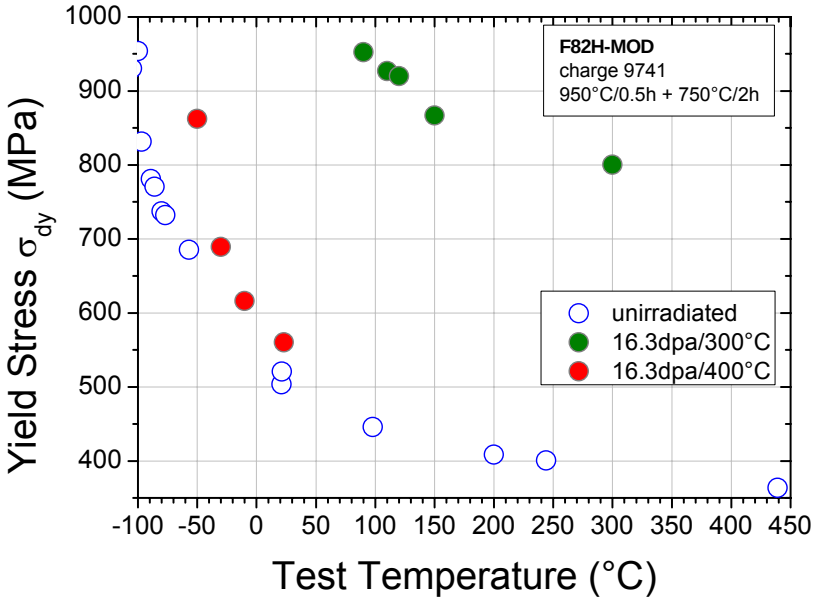

Fig. 8-6 Dynamic yield stress vs. test temperature for unirradiated and 16.3 dpa (average) irradiated F82H-mod.

Irradiation condition: unirradiated

Specimen	Test Temperature (°C)	Impact Energy (J)	Yield Stress (MPa)
BO755	-105	0.50	930
BO754	-100	0.72	954
B0745	-97	4.31	831
BO753	-89	0.38	781
B0744	-86	7.35	770
BO752	-80	8.00	737
B0743	-77	9.58	732
B0742	-57	9.40	685
B0741	21	9.35	504
BO751	21	9.66	521
B0746	98	9.18	446
BO756	200	8.60	408
B0747	244	8.08	401
B0748	439	7.30	364

Irradiation condition: 16.3dpa/300°C

Specimen	Test Temperature (°C)	Impact Energy (J)	Yield Stress (MPa)
YF02	90	0.91	953
YF03	110	5.92	927
YF04	120	4.26	920
YF01	150	6.74	867
YF05	300	6.08	800

Irradiation condition: 16.3dpa/400°C

Specimen	Test Temperature (°C)	Impact Energy (J)	Yield Stress (MPa)
YF09	-50	0.96	862
YF08	-30	8.08	689
YF07	-10	9.23	616
YF06	23	9.34	561

Evaluation:

Irradiation Condition	USE (J)	DBTT (°C)	LTUS (°C)	σ_{RT} (MPa)	σ_{100} (MPa)
unirradiated	9.66	-86	-77	512	439
16.3dpa/300°C	6.74	110	150	-	920
16.3dpa/400°C	9.34	-34	-10	560	-

Irradiation Condition	ΔUSE (%)	ΔDBTT (°C)	$\Delta\sigma_{RT}$ (MPa)	$\Delta\sigma_{100}$ (MPa)
16.3dpa/300°C	-30	196	-	481
16.3dpa/400°C	-3	52	48	-

8.3.4 OPTIFER-Ia

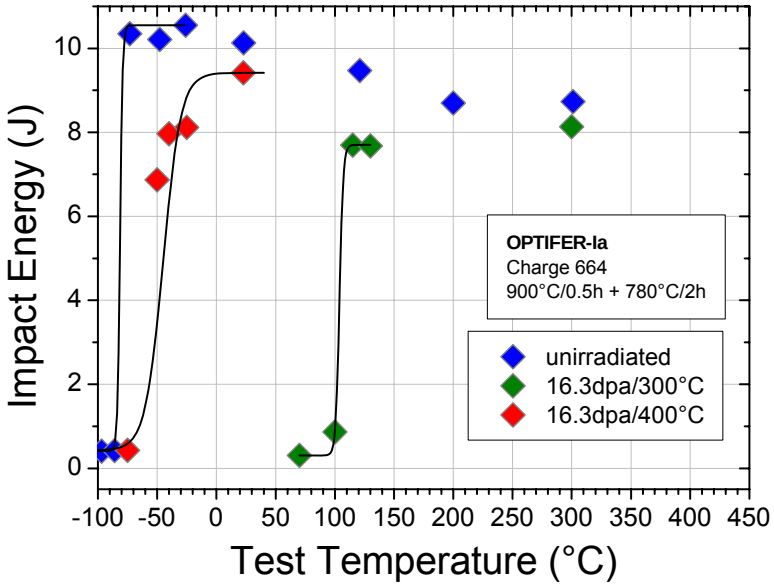

Fig. 8-7 Charpy impact energy vs. test temperature for unirradiated and 16.3 dpa (average) irradiated OPTIFER-Ia. The solid lines are fits according to Eq. (2-1).

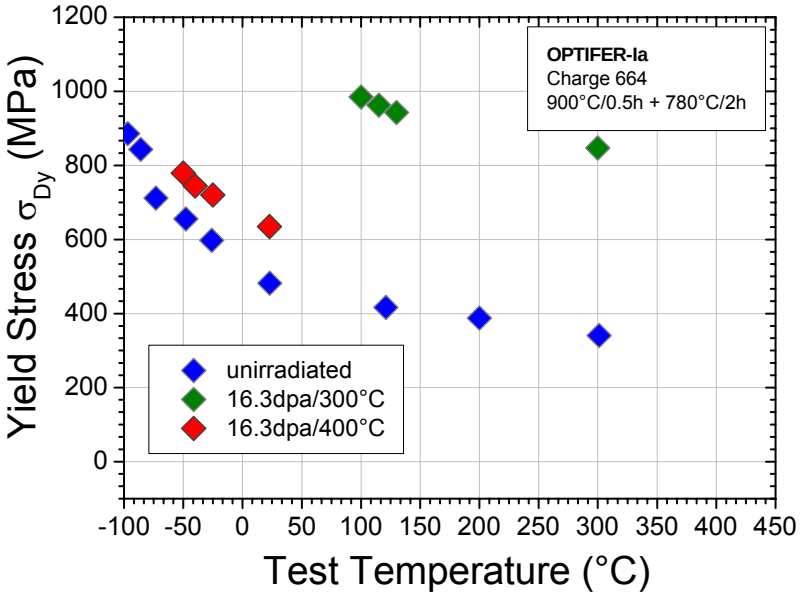

Fig. 8-8 Dynamic yield stress vs. test temperature for unirradiated and 16.3 dpa (average) irradiated OPTIFER-Ia.

Irradiation condition: unirradiated

Specimen	Test Temperature (°C)	Impact Energy (J)	Yield Stress (MPa)
XD39	-97	0.41	886
XD40	-86	0.42	843
XD38	-73	10.35	712
XD37	-48	10.21	655
XD36	-26	10.55	598
XD41	23	10.13	482
XD42	121	9.47	416
XD43	200	8.70	387
XD44	301	8.73	340

Irradiation condition: 16.3dpa/300°C

Specimen	Test Temperature (°C)	Impact Energy (J)	Yield Stress (MPa)
YK01	70	0.31	-
YK02	100	0.87	984
YK04	115	7.69	963
YK03	130	7.68	943
YK05	300	8.14	847

Irradiation condition: 16.3dpa/400°C

Specimen	Test Temperature (°C)	Impact Energy (J)	Yield Stress (MPa)
YK08	-75	0.43	0
YK07	-50	6.87	780
YK06	-40	7.97	744
YK09	-25	8.12	720
YK10	23	9.42	635

Evaluation:

Irradiation Condition	USE (J)	DBTT (°C)	LTUS (°C)	σ_{RT} (MPa)	σ_{100} (MPa)
unirradiated	10.55	-81	-77	482	416
16.3dpa/300°C	8.14	104	115	-	963
16.3dpa/400°C	9.42	-45	23 (-48)	635	-

The brackets next to LTUS for 16.3dpa/400°C show the corresponding uncertainty.

Irradiation Condition	ΔUSE (%)	ΔDBTT (°C)	$\Delta\sigma_{RT}$ (MPa)	$\Delta\sigma_{100}$ (MPa)
16.3dpa/300°C	-23	185	-	547
16.3dpa/400°C	-11	36	153	-

8.3.5 GA3X

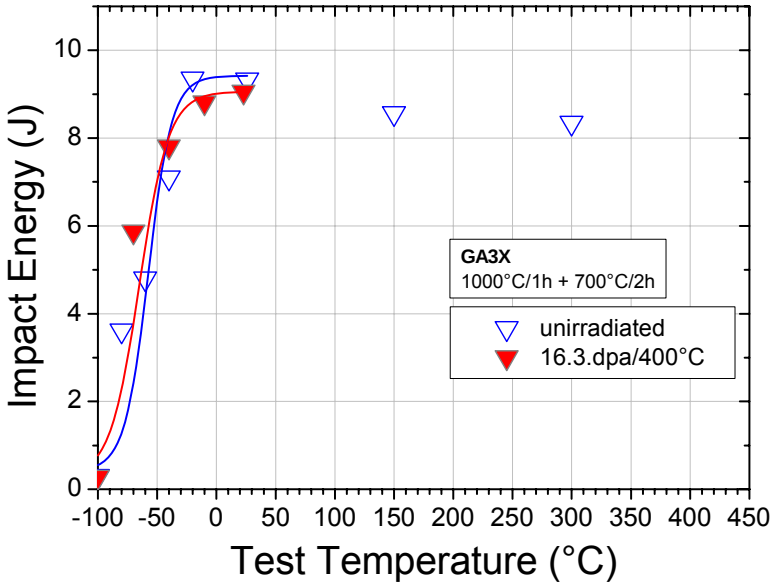

Fig. 8-9 Charpy impact energy vs. test temperature for unirradiated and 16.3 dpa (average) irradiated GA3X. The solid lines are fits according to Eq. (2-1).

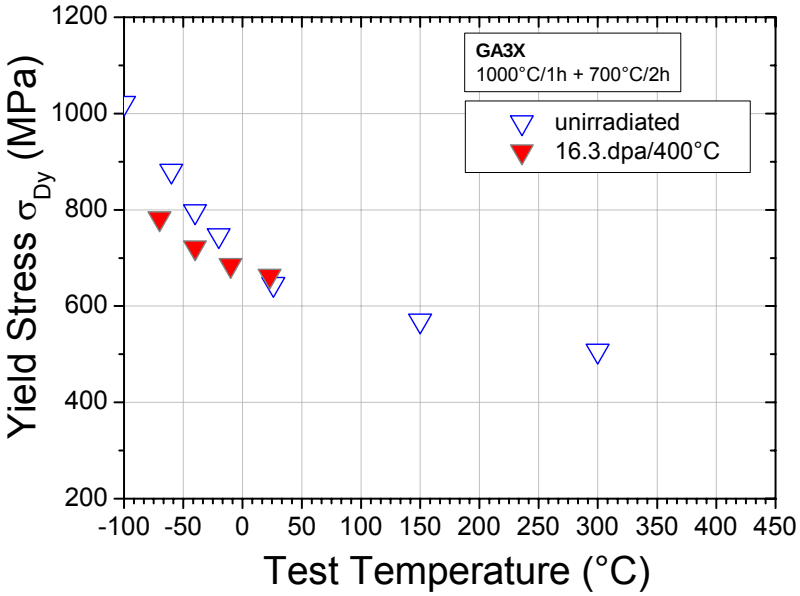

Fig. 8-10 Dynamic yield stress vs. test temperature for unirradiated and 16.3 dpa (average) irradiated GA3X.

Irradiation condition: unirradiated

Specimen	Test Temperature (°C)	Impact Energy (J)	Yield Stress (MPa)
Q06	-100	0.3	1022
Q05	-80	3.62	-
Q04	-60	4.8	881
Q03	-40	7.1	797
Q02	-20	9.35	747
Q01	26	9.33	646
Q07	150	8.57	570
Q08	300	8.35	507

Irradiation condition: 16.3dpa/400°C

Specimen	Test Temperature (°C)	Impact Energy (J)	Yield Stress (MPa)
YX04	-100	0.28	0
YX03	-70	5.87	782
YX02	-40	7.81	722
YX05	-10	8.81	685
YX01	23	9.06	663

Evaluation:

Irradiation Condition	USE (J)	DBTT (°C)	LTUS (°C)	σ_{RT} (MPa)	σ_{100} (MPa)
unirradiated	9.35	-58	-20	652	601
16.3dpa/400°C	9.06	-65	-10	663	-

Irradiation Condition	ΔUSE (%)	ΔDBTT (°C)	$\Delta\sigma_{RT}$ (MPa)
16.3dpa/400°C	-3	-7	8

8.3.6 MANET-I

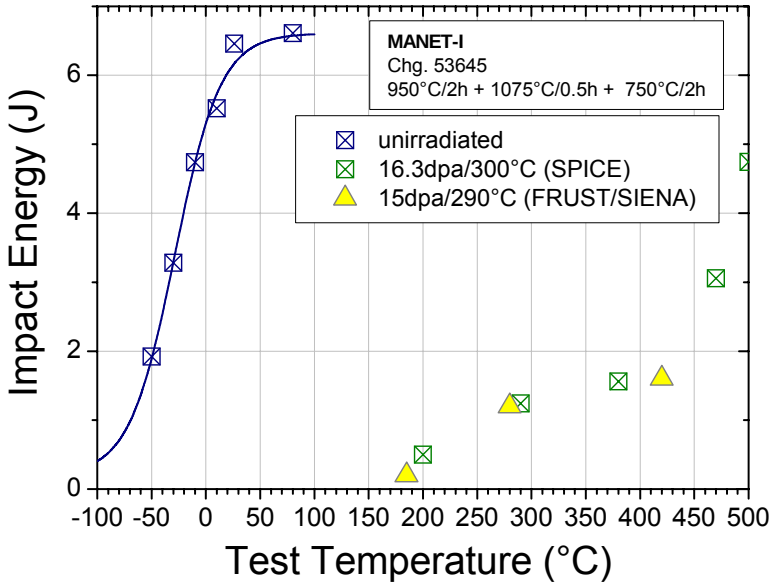

Fig. 8-11 Charpy impact energy vs. test temperature for unirradiated and 16.3dpa/300°C (SPICE) and 15dpa/290°C (FRUST/SIENA [1]) irradiated MANET-I. The solid line is fit to unirradiated condition according to Eq. (2-1).

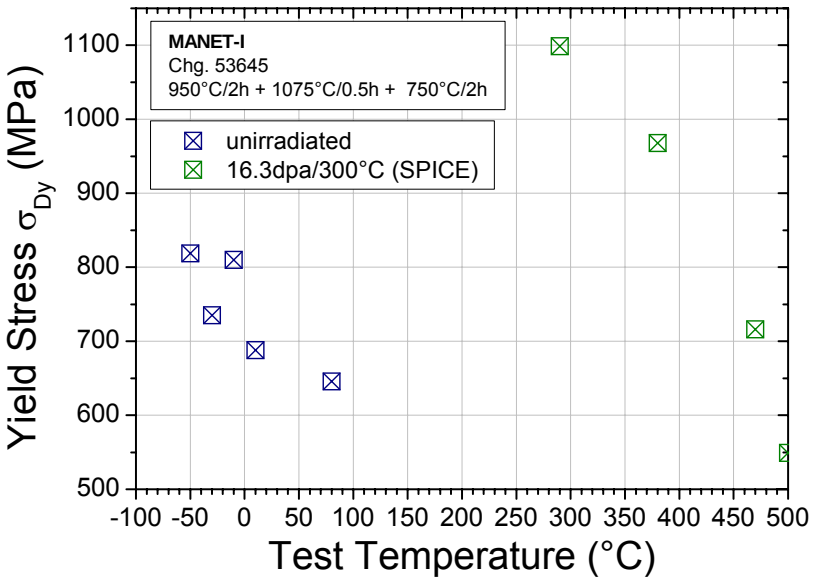

Fig. 8-12 Dynamic yield stress vs. test temperature for unirradiated and 16.3 dpa (average) irradiated MANET-I.

Irradiation condition: unirradiated

Specimen	Test Temperature (°C)	Impact Energy (J)	Yield Stress (MPa)
G05	-50	1.92	819
G04	-30	3.28	735
G03	-10	4.74	810
G06	10	5.52	688
G02	26	6.46	-
G01	80	6.61	646

Irradiation condition: 16.3dpa/300°C

Specimen	Test Temperature (°C)	Impact Energy (J)	Yield Stress (MPa)
YS05	200	0.50	-
YS01	290	1.24	1099
YS03	380	1.56	968
YS04	470	3.06	716
YS02	500	4.74	549

Evaluation:

Irradiation Condition	USE (J)	DBTT (°C)	LTUS (°C)	σ_{100} (MPa)
unirradiated	6.61	-30	20	640
16.3dpa/300C	4.74	446	500	-

Irradiation Condition	ΔUSE (%)	ΔDBTT (°C)
16.3dpa/300°C	-28	476

8.3.7 ODS EUROFER

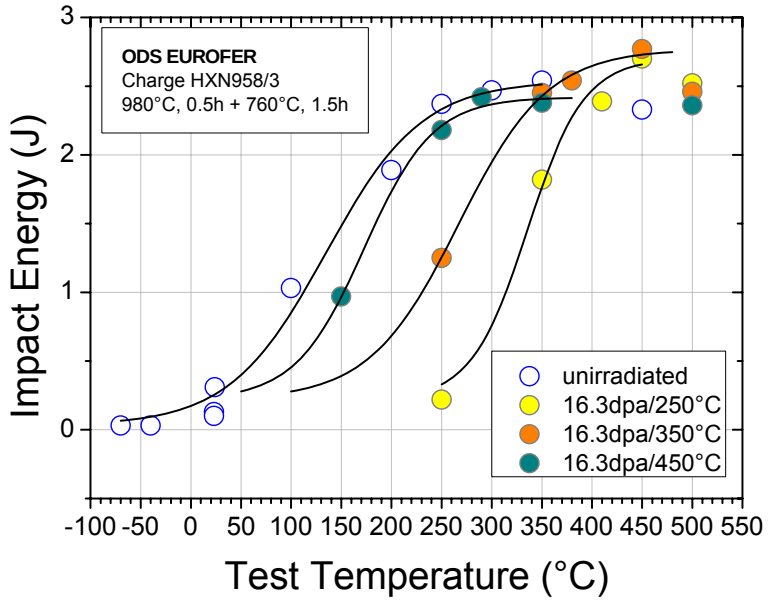

Fig. 8-13 Charpy impact energy vs. test temperature for unirradiated and 16.3 dpa (average) irradiated ODS EUROFER. The solid lines are fits according to Eq. (2-1).

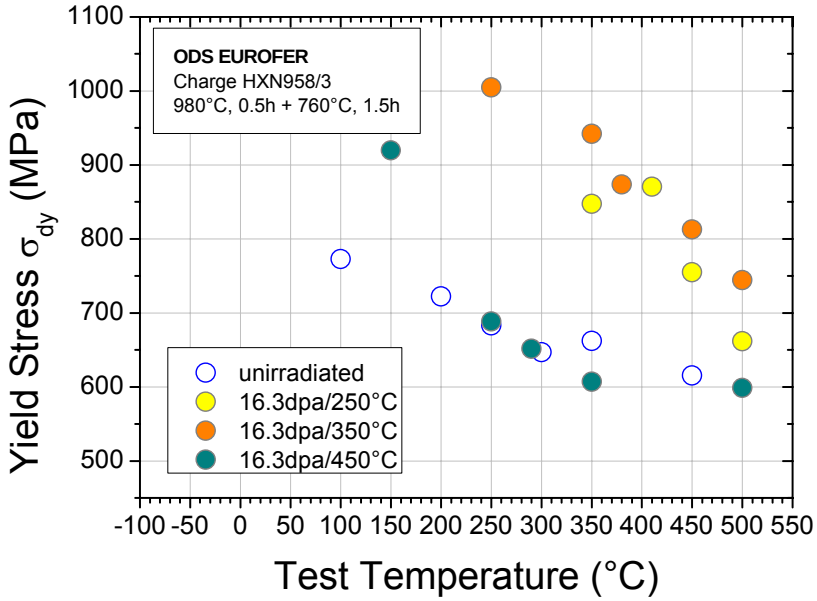

Fig. 8-14 Dynamic yield stress vs. test temperature for unirradiated and 16.3 dpa (average) irradiated ODS EUROFER.

Irradiation condition: unirradiated

Specimen	Test Temperature (°C)	Impact Energy (J)	Yield Stress (MPa)
EOU03	-70	0.03	-
EOU02	-40	0.03	-
EOU01	23	0.13	-
EO11	23	0.1	-
EO10	24	0.31	-
EOU04	100	1.03	773
EOU05	200	1.89	723
EOU07	250	2.37	683
EOU06	300	2.47	647
EOU08	350	2.54	662
EOU09	450	2.33	616

Irradiation condition: 16.3dpa/250°C

Specimen	Test Temperature (°C)	Impact Energy (J)	Yield Stress (MPa)
YH12	250	0.22	-
YH13	350	1.82	847
YH14	410	2.39	871
YH11	450	2.7	755
YH15	500	2.52	662

Irradiation condition: 16.3dpa/350°C

Specimen	Test Temperature (°C)	Impact Energy (J)	Yield Stress (MPa)
YH09	250	1.25	1005
YH10	350	2.45	942
YH07	380	2.54	874
YH06	450	2.77	813
YH08	500	2.46	744

Irradiation condition: 16.3dpa/450°C

Specimen	Test Temperature (°C)	Impact Energy (J)	Yield Stress (MPa)
YH02	150	0.97	920
YH01	250	2.18	689
YH04	290	2.42	652
YH03	350	2.38	607
YH05	500	2.36	599

Evaluation:

Irradiation Condition	USE (J)	DBTT (°C)	LTUS (°C)	σ_{350} (MPa)
unirradiated	2.54	135	250	662
16.3dpa/250°C	2.70	336	410	847
16.3dpa/350°C	2.77	267	380	942
16.3dpa/450°C	2.42	173	290	607

Irradiation Condition	ΔUSE (%)	ΔDBTT (°C)	$\Delta\sigma_{350}$ (MPa)
250	6	201	185
350	9	132	280
450	-5	38	-55

8.3.8 ADS2

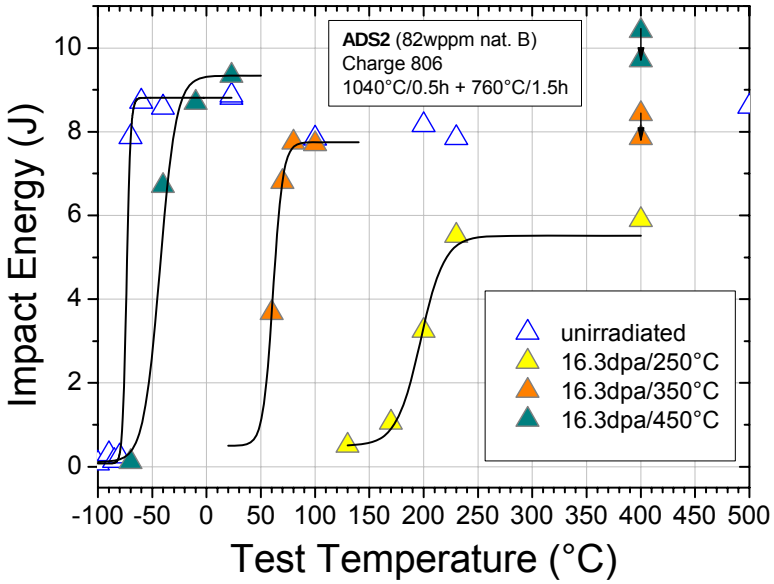

Fig. 8-15 Charpy impact energy vs. test temperature for unirradiated and 16.3 dpa (average) irradiated ADS2. The solid lines are fits according to Eq. (2-1). Vertical arrows indicate reduced energy values after correction the clamping of the specimens between the supporters.

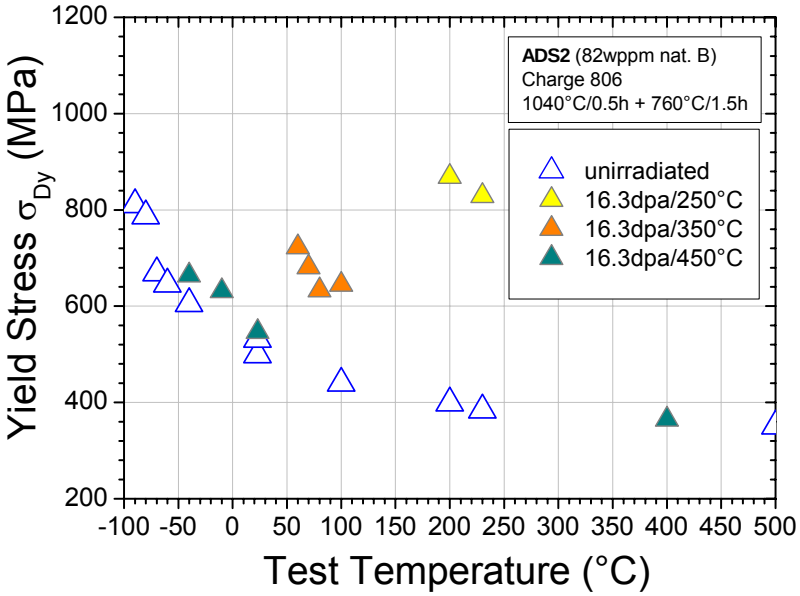

Fig. 8-16 Dynamic yield stress vs. test temperature for unirradiated and 16.3 dpa (average) irradiated ADS2.

Irradiation condition: unirradiated

Specimen	Test Temperature (°C)	Impact Energy (J)	Yield Stress (MPa)
A2U06	-100	0.08	-
A2U05	-90	0.3	811
A2U08	-85	0.14	-
A2U04	-80	0.25	787
A2U03	-70	7.87	670
A2U07	-60	8.72	646
A2U02	-40	8.58	605
A2U01	23	8.81	499
A2U13	23	8.87	531
A2U09	100	7.84	440
A2U10	200	8.16	399
A2U11	230	7.85	384
A2U12	500	8.60	351

Irradiation condition: 16.3dpa/250°C

Specimen	Test Temperature (°C)	Impact Energy (J)	Yield Stress (MPa)
YC01	130	0.50	-
YC02	170	1.06	-
YC03	200	3.25	869
YC04	230	5.52	829
YC05	400	5.89	-

Irradiation condition: 16.3dpa/350°C

Specimen	Test Temperature (°C)	Impact Energy (J)	Yield Stress (MPa)
YC06	60	3.67	723
YC10	70	6.80	681
YC08	80	7.75	633
YC07	100	7.70	645
YC09	400	8.42 (7.85)	-

Energy value after correction the clamping of the specimen between the supporters is shown in brackets.

Irradiation condition: 16.3dpa/450°C

Specimen	Test Temperature (°C)	Impact Energy (J)	Yield Stress (MPa)
YC12	-70	0.11	-
YC11	-40	6.71	664
YC13	-10	8.69	631
YC15	23	9.34	547
YC14	400	10.41 (9.71)	365

Energy value after correction the clamping of the specimen between the supporters is shown in brackets.

Evaluation:

Irradiation Condition	USE (J)	DBTT (°C)	LTUS (°C)	σ_{RT} (MPa)	σ_{100} (MPa)
unirradiated	8.81	-74	-70	499	440
16.3dpa/250°C	5.52	197	230	-	
16.3dpa/350°C	7.75	61	70	-	645
16.3dpa/450°C	9.34	-43	-10	547	-

Irradiation Condition	ΔUSE (%)	ΔDBTT (°C)	$\Delta\sigma_{RT}$ (MPa)	$\Delta\sigma_{100}$ (MPa)
16.3dpa/250°C	-37	271	-	-
16.3dpa/350°C	-12	135	-	205
16.3dpa/450°C	6	31	48	-

8.3.9 ADS3

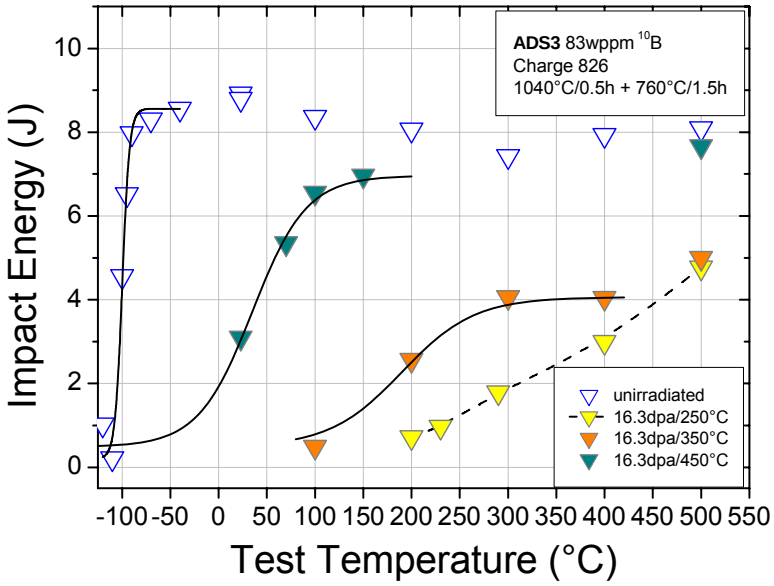

Fig. 8-17 Charpy impact energy vs. test temperature for unirradiated and 16.3 dpa (average) irradiated ADS3. The solid lines are fits according to Eq. (2-1). The dashed line is a eye guide only.

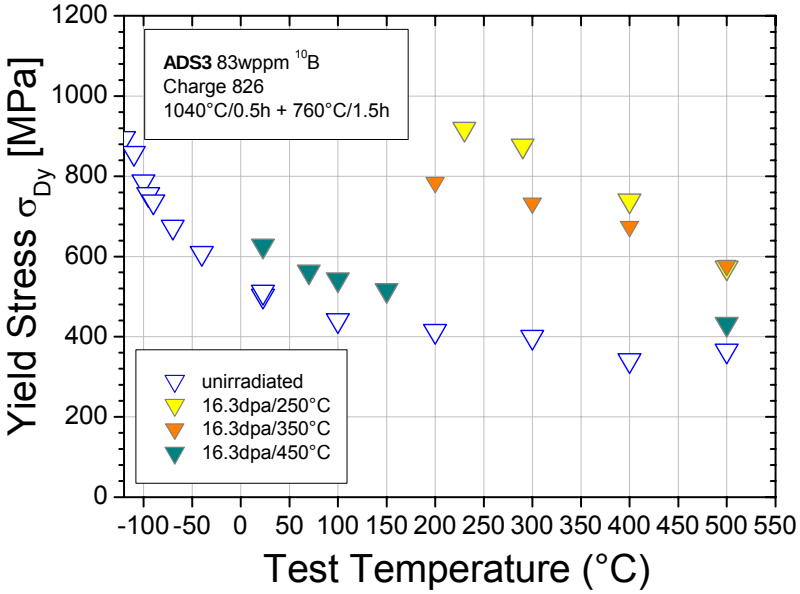

Fig. 8-18 Dynamic yield stress vs. test temperature for unirradiated and 16.3 dpa (average) irradiated ADS3.

Irradiation condition: unirradiated

Specimen	Test Temperature (°C)	Impact Energy (J)	Yield Stress (MPa)
A3U06	-120	1.02	895
A3U08	-110	0.21	858
A3U05	-100	4.56	787
A3U07	-95	6.52	756
A3U04	-90	7.97	737
A3U03	-70	8.30	674
A3U02	-40	8.56	609
A3U01	23	8.92	502
A3U13	23	8.79	512
A3U09	100	8.36	441
A3U10	200	8.06	414
A3U11	300	7.43	400
A3U12	400	7.93	341
A3U14	500	8.09	365

Irradiation condition: 16.3dpa/250°C

Specimen	Test Temperature (°C)	Impact Energy (J)	Yield Stress (MPa)
YD01	200	0.72	
YD02	230	0.97	919
YD03	290	1.79	877
YD04	400	2.99	739
YD05	500	4.77	572

Irradiation condition: 16.3dpa/350°C

Specimen	Test Temperature (°C)	Impact Energy (J)	Yield Stress (MPa)
YD09	100	0.49	
YD06	200	2.56	784
YD07	300	4.06	733
YD08	400	4.04	674
YD10	500	5.00	578

Irradiation condition: 16.3dpa/450°C

Specimen	Test Temperature (°C)	Impact Energy (J)	Yield Stress (MPa)
YD11	23	3.09	627
YD14	70	5.35	562
YD12	100	6.55	543
YD13	150	6.96	516
YD15	500	7.66	432

Evaluation:

Irradiation Condition	USE (J)	DBTT (°C)	LTUS (°C)	σ_{RT} (MPa)	σ_{100} (MPa)
unirradiated	8.92	-100	-70	502	441
16.3dpa/250°C	2.99 (+1.78)	270 (+75)	400	-	-
16.3dpa/350°C	4.06	190	300	-	-
16.3dpa/450°C	6.96	35	100	627	543

The brackets next to USE and DBTT for 16.3dpa/250°C show the corresponding uncertainties.

Irradiation Condition	ΔUSE (%)	ΔDBTT (°C)	$\Delta\sigma_{RT}$ (MPa)	$\Delta\sigma_{100}$ (MPa)
250	-66 (+20)	370 (+75)	-	-
350	-54	290	-	-
450	-22	135	125	102

The brackets next to ΔUSE and ΔDBTT for 16.3dpa/250°C show the corresponding uncertainties.

8.3.10 ADS4

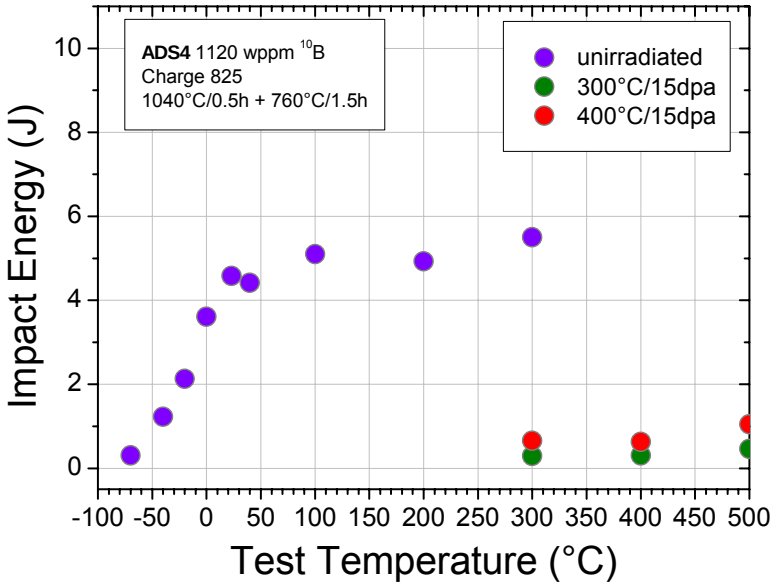

Fig. 8-19 Charpy impact energy vs. test temperature for unirradiated and 16.3 dpa (average) irradiated ADS4.

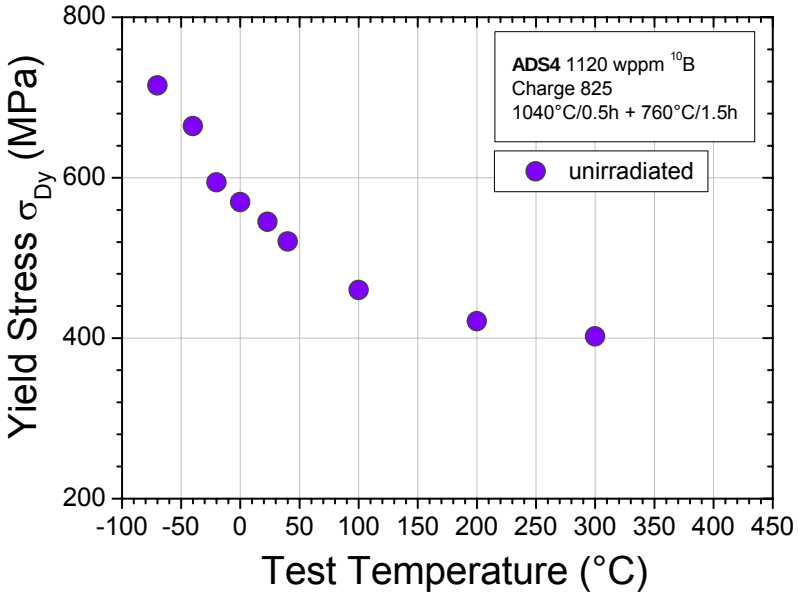

Fig. 8-20 Dynamic yield stress vs. test temperature for unirradiated ADS4.

Irradiation condition: unirradiated

Specimen	Test Temperature (°C)	Impact Energy (J)	Yield Stress (MPa)
A4U03	-70	0.31	715
A4U02	-40	1.23	664
A4U05	-20	2.13	594
A4U04	0	3.61	570
A4U01	23	4.58	545
A4U07	40	4.42	521
A4U06	100	5.10	460
A4U08	200	4.93	421
A4U09	300	5.50	402

Irradiation condition: 16.3dpa/300°C

Specimen	Test Temperature (°C)	Impact Energy (J)
YE01	300	0.29
YE02	400	0.31
YE03	500	0.46

Irradiation condition: 16.3dpa/400°C

Specimen	Test Temperature (°C)	Impact Energy (J)
YE06	300	0.659
YE07	400	0.63
YE08	500	1.05

Evaluation:

Irradiation Condition	USE (J)	DBTT (°C)	LTUS (°C)	σ_{RT} (MPa)	σ_{100} (MPa)
unirradiated	5.50	-12	40	545	460